

Signature of 2HDM at Higgs Factories

WENHAI XIE^{1,4*}, R. BENBRIK^{2†}, ABDELJALIL HABJIA^{3‡}, BIN GONG^{1§}, QI-SHU
YAN^{4,5¶},

¹ *Theory Division, Institute of High Energy Physics, Chinese Academy of Sciences, Beijing 100049, China.*

² *MSISM Team, Faculté Polydisciplinaire de Safi, Sidi Bouzid, B.P. 4162, Safi, Morocco*

³ *LISRT Beni-Mellal, Morocco*

⁴ *School of Physics Sciences, University of Chinese Academy of Sciences, Beijing 100049, China*

⁵ *Center for Future High Energy Physics, Chinese Academy of Sciences, Beijing 100049, China*

Abstract

The full one-loop corrections, both the weak and QED corrections, to the process $e^+e^- \rightarrow Z\phi$ ($\phi = h^0, H^0$) at the Higgs factories are presented. Up to the $O(\alpha_{EM})$ level, the virtual corrections are evaluated in a Feynman-diagrammatic approach. The real emission corrections are computed using Feynman Diagram Calculation (FDC) system and the collinear divergences are regularized by the structure functions of electron. Using the FDC system, we study the corrections both in the SM and the two Higgs doublet model (2HDM), respectively. After taking into account experimental constraints from the current LHC data, we propose four interesting benchmark scenarios of 2HDM for future colliders. By using these benchmark scenarios, we evaluate the deviation of $\Delta\sigma(e^+e^- \rightarrow Z\phi)$ from their Standard Model (SM) values. We also examine $\phi \rightarrow b\bar{b}$ and $\phi \rightarrow \tau^+\tau^-$, which may receive large EW contribution from triple Higgs couplings which are absent in the SM. It is found that for these benchmark scenarios, both EW and real emission corrections are sizable and could be measured at a future e^+e^- collider such as the ILC, CLIC and CEPC.

*xiewh@ihep.ac.cn

†r.benbrik@uca.ac.ma

‡ahabjia@gmail.com

§twain@ihep.ac.cn

¶yanqishu@ucas.ac.cn

1 Introduction

A Higgs-like boson (h) has been discovered in the first Run of the Large Hadron Collider (LHC) in 2012 [1, 2]. Based on the data of Run-1, ATLAS and CMS collaborations has established Higgs boson mass with $m_h = 125.09 \pm 0.21$ (stat.) ± 0.11 (syst.) GeV [3]. LHC also performed several Higgs coupling measurements to a precision around 10 – 20%, such as Higgs couplings to dibosons VV with $V = W^\pm, Z, \gamma$. Very recently, LHC have also measured Higgs couplings to the fermions of the third generation over 5σ , via the process $pp \rightarrow Vh(h \rightarrow b\bar{b})$ [4, 5], via the VBF process $pp \rightarrow jjh(h \rightarrow \tau^+\tau^-)$ [6, 7], and $pp \rightarrow tth$ with combined Higgs boson decay final states [8, 9]. These measurements demonstrated that the SM works quite well in the current Higgs data.

One of the tasks of the LHC Run-2 at 13 TeV (and 14 TeV) with High Luminosity (HL) would be to improve all the aforementioned measurements and to perform new ones such as accessing $h \rightarrow \gamma Z$ as well as the triple self-coupling of the Higgs boson. It is expected that the new LHC Run-2 will pin down the uncertainty in $h \rightarrow b\bar{b}$ and $h \rightarrow \tau^+\tau^-$ to 10-13% and 6-8% for bottom quarks and tau leptons, respectively. These measurements will be further ameliorated by the High Luminosity option for the LHC (HL-LHC) down to uncertainties of 4-7% for b quarks and 2-5% for τ leptons [12]. Moreover, in the clean environment of the e^+e^- Linear Collider (LC), which can act as a Higgs factory, the uncertainties on $h \rightarrow b\bar{b}$ and $h \rightarrow \tau^+\tau^-$ would be much smaller reaching 0.6% for the couplings in $h^0 \rightarrow b\bar{b}$ and 1.3% for those in $h^0 \rightarrow \tau^+\tau^-$ [13, 14].

The above accuracies on fermionic Higgs decay measurements, if reached, are of the size comparable to the effects of radiative corrections to some Higgs decays. Therefore, one can use these radiative correction effects to distinguish between the Standard Model (SM) and various beyond-standard models (BSM). In this respect, precise calculations of Higgs-boson production and decay rates have been performed already quite some time ago with great achievements (see e.g. [15, 16]). QCD corrections to Higgs decays into quarks are very well known up to $\mathcal{O}(\alpha_s^3)$ as well as additional corrections at $\mathcal{O}(\alpha_s^2)$ that involve logarithms of the light-quark masses and also heavy top contributions [15]. Electroweak radiative corrections to fermionic decays ($b\bar{b}$ and $\tau^+\tau^-$) of the Higgs boson in the SM are also well established [17–19] in the on-shell scheme. In the framework of the Two-Higgs-Doublet Model (2HDM), several studies have been carried out to evaluate the electroweak corrections to fermionic Higgs decays [20, 21]. The calculation of Ref. [20] is done in the on-shell scheme except for the Higgs field renormalization where the $\overline{\text{MS}}$ subtraction has been used, while the one of Ref. [21] is performed using the on-shell renormalization scheme of [22].

At the LHC, due to the large theoretical uncertainties like the PDF and large experimental background, the precision measurements of the Higgs boson are rather challenging. In contrast, e^+e^- colliders can offer us precision measurements on the production and decay properties of Higgs boson. At an 240 GeV e^+e^- collider, the Higgs-strahlung process $e^+e^- \rightarrow Zh$ is the dominant production channel for the Higgs boson, for which properties of Higgs boson can be reconstructed by using the recoiled Z boson via its leptonic decay. For a center-of-mass energy of 240-250 GeV and an integrated luminosity of 250 fb^{-1} , $\mathcal{O}(10^5)$

Higgs bosons per year will be produced which can lead to a measurement of the Higgs couplings at percent level [23–25]. At the international linear collider (ILC) experiments [26], the luminosity is expected to be high and a quite small experimental error is expected. Correspondingly, precise theoretical predictions to the physical observables related to Higgs boson are required.

In this work, we will propose a few benchmark scenarios of 2HDM after taking into account theoretical constraints as well as experimental restrictions from recent LHC data. By using these benchmark scenarios, we will study the effects of electroweak radiative corrections to the production process $e^+e^- \rightarrow Z\phi$ and the decay processes $\phi \rightarrow b\bar{b}$ and $\phi \rightarrow \tau^+\tau^-$. We will also report our full next leading order calculation on the cross section of $e^+e^- \rightarrow Z\phi$ with $\phi = h^0, H^0$ in 2HDM by including both virtual correction up to one-loop and real emission of a photon. Our results are consistent with those given in the previous work [27] under the same setting of 2HDM parameters. The complete SM 1-loop correction of $\sigma(e^+e^- \rightarrow Zh_{SM})$ have already been calculated using the GRACE [28] and we reproduced the results for comparison. We noticed that the EW corrections of new physics in our benchmark scenarios can be of order $-10\% \sim -20\%$ even after taking into account the recent constraints LHC data. While the contribution of real emission has positive sign.

To examine the deviation caused by the new physics, we will also evaluate the ratio of branching fractions of Higgs decays in the 2HDM [29, 30],

$$\Delta_{ff}(\phi) = \frac{\Gamma_1^{2HDM}(\phi \rightarrow f\bar{f})}{\Gamma_1^{SM}(h \rightarrow f\bar{f})} - 1, \quad (1)$$

This ratio of Higgs boson decay widths is independent of the production process, but it is sensitive to the electroweak corrections of new physics that may not affect the production rate of Higgs bosons. This ratio is less sensitive to the systematic errors (which drop out in the ratio) so it could be useful to discriminate the SM against other models such as 2HDM or supersymmetric models.

The paper is organized as follows. In section 2, we review the Yukawa textures, scalar potential and Higgs self-couplings of the 2HDM model, as well as the theoretical and experimental constraints on the model. In section 3, we outline the framework of our calculation and specifies the renormalization scheme we will use. In section 4, we present the numerical results. We conclude this work in section 5.

2 The 2HDM model

2.1 Yukawa textures

In the 2HDM, fermion and gauge boson masses are generated from two Higgs doublets $\Phi_{1,2}$ where both of them acquire vacuum expectation values $v_{1,2}$. If both Higgs fields couple to all fermions, Flavor Changing Neutral Currents (FCNC) are generated which can invalidate some low energy observables in B, D and K physics. In order to avoid such FCNC, the Paschos-Glashow-Weinberg theorem [31] proposes a Z_2 symmetry that forbids FCNC couplings at the tree level. Depending on the Z_2 assignment, we have four type of models [16, 32].

| type | $\xi_u^{h^0}$ | $\xi_d^{h^0}$ | $\xi_l^{h^0}$ | $\xi_u^{H^0}$ | $\xi_d^{H^0}$ | $\xi_l^{H^0}$ | $\xi_u^{A^0}$ | $\xi_d^{A^0}$ | $\xi_l^{A^0}$ |
|------|--------------------|---------------------|---------------------|--------------------|--------------------|--------------------|---------------|---------------|---------------|
| I | c_α/s_β | c_α/s_β | c_α/s_β | s_α/s_β | s_α/s_β | s_α/s_β | $\cot \beta$ | $-\cot \beta$ | $-\cot \beta$ |
| II | c_α/s_β | $-s_\alpha/c_\beta$ | $-s_\alpha/c_\beta$ | s_α/s_β | c_α/c_β | c_α/c_β | $\cot \beta$ | $\tan \beta$ | $\tan \beta$ |
| III | c_α/s_β | c_α/s_β | $-s_\alpha/c_\beta$ | s_α/s_β | s_α/s_β | c_α/c_β | $\cot \beta$ | $-\cot \beta$ | $\tan \beta$ |
| IV | c_α/s_β | $-s_\alpha/c_\beta$ | c_α/s_β | s_α/s_β | c_α/c_β | s_α/s_β | $\cot \beta$ | $\tan \beta$ | $-\cot \beta$ |

Table 1: Yukawa coupling coefficients of the neutral Higgs bosons h^0 , H^0 , A^0 to the up-quarks, down-quarks and the charged leptons (u, d, ℓ) in the four 2HDM types.

In the 2HDM type-I model, only the second doublet Φ_2 interacts with all the fermions like in SM. In 2HDM type-II model the doublet Φ_2 interacts with up-type quarks and Φ_1 interacts with the down-type quarks and charged leptons. In 2HDM type-III, charged leptons couple to Φ_1 while all the quarks couple to Φ_2 . Finally, in 2HDM type IV, charged leptons and up-type quarks couple to Φ_2 while down-type quarks acquire masses from their couplings to Φ_1 . The most general Yukawa interactions can be written as follows,

$$-\mathcal{L}_{\text{Yukawa}}^{\text{2HDM}} = \overline{Q}_L Y_u \tilde{\Phi}_2 u_R + \overline{Q}_L Y_d \Phi_d d_R + \overline{L}_L Y_\ell \Phi_\ell \ell_R + \text{h.c.}, \quad (2)$$

where $\Phi_{d,l}$ ($d, l = 1, 2$) represents Φ_1 or Φ_2 and Y_f ($f = u, d$ or ℓ) stands for Yukawa matrices. The two complex scalar $SU(2)$ doublets can be decomposed according to

$$\Phi_i = \begin{pmatrix} \phi_i^+ \\ (v_i + \rho_i + i\eta_i)/\sqrt{2} \end{pmatrix}, \quad i = 1, 2, \quad (3)$$

where $v_{1,2}$ are the vacuum expectation values of $\Phi_{1,2}$. The mass eigenstates for the Higgs bosons are obtained by orthogonal transformations,

$$\begin{pmatrix} \phi_1^\pm \\ \phi_2^\pm \end{pmatrix} = R_\beta \begin{pmatrix} G^\pm \\ H^\pm \end{pmatrix}, \quad \begin{pmatrix} \rho_1 \\ \rho_2 \end{pmatrix} = R_\alpha \begin{pmatrix} H^0 \\ h^0 \end{pmatrix}, \quad \begin{pmatrix} \eta_1 \\ \eta_2 \end{pmatrix} = R_\beta \begin{pmatrix} G^0 \\ A^0 \end{pmatrix}, \quad (4)$$

with the generic orthogonal matrix

$$R_\theta = \begin{pmatrix} \cos \theta & -\sin \theta \\ \sin \theta & \cos \theta \end{pmatrix}.$$

From the eight fields initially present in the two scalar doublets, three of them, namely the Goldstone bosons G^\pm and G^0 , are eaten by the longitudinal components of W^\pm and Z , respectively. The remaining five are physical Higgs fields, two CP-even H^0 and h^0 , a CP-odd A^0 , and a pair of charged scalars H^\pm .

Writing the Yukawa interactions eq. (2) in terms of mass eigenstates of the neutral and charged Higgs bosons yields

$$\begin{aligned}
-\mathcal{L}_{\text{Yukawa}}^{2\text{HDM}} = & \sum_{f=u,d,\ell} \frac{m_f}{v} \left(\xi_f^{h^0} \bar{f} f h^0 + \xi_f^{H^0} \bar{f} f H^0 - i \xi_f^{A^0} \bar{f} \gamma_5 f A^0 \right) \\
& + \left\{ \frac{\sqrt{2} V_{ud}}{v} \bar{u} \left(m_u \xi_u^{A^0} P_L + m_d \xi_d^{A^0} P_R \right) d H^+ + \frac{\sqrt{2} m_\ell \xi_\ell^{A^0}}{v} \bar{\nu}_L \ell_R H^+ + \text{h.c.} \right\},
\end{aligned} \tag{5}$$

where $v^2 = v_1^2 + v_2^2 = (\sqrt{2} G_F)^{-1}$; P_R and P_L are the right- and left-handed projection operators, respectively. The coefficients $\xi_f^{h^0}$, $\xi_f^{H^0}$ and $\xi_f^{A^0}$ ($f = u, d, l$) in the four 2HDM types are given in the Table 1.

2.2 Scalar potential and self-coupling of the Higgs bosons

The most general 2HDM scalar potential which is invariant under $SU(2)_L \otimes U(1)_Y$ and possesses a soft Z_2 breaking term (m_{12}^2) [16, 32, 33] can be written in the following way,

$$\begin{aligned}
V_{2\text{HDM}} = & m_{11}^2 \Phi_1^\dagger \Phi_1 + m_{22}^2 \Phi_2^\dagger \Phi_2 - m_{12}^2 \left(\Phi_1^\dagger \Phi_2 + \Phi_2^\dagger \Phi_1 \right) + \frac{\lambda_1}{2} (\Phi_1^\dagger \Phi_1)^2 + \frac{\lambda_2}{2} (\Phi_2^\dagger \Phi_2)^2 \\
& + \lambda_3 (\Phi_1^\dagger \Phi_1) (\Phi_2^\dagger \Phi_2) + \lambda_4 \left| \Phi_1^\dagger \Phi_2 \right|^2 + \frac{\lambda_5}{2} \left\{ \left(\Phi_1^\dagger \Phi_2 \right)^2 + \left(\Phi_2^\dagger \Phi_1 \right)^2 \right\}.
\end{aligned} \tag{6}$$

Hermiticity of the potential requires m_{11}^2 , m_{22}^2 and $\lambda_{1,2,3,4}$ to be real, while m_{12}^2 and λ_5 could be complex in case one would allow for CP violation in the Higgs sector. In what follows we assume that there is no CP violation, which means m_{12}^2 and λ_5 are taken as real.

From the above potential, Eq. (6), we can derive the triple Higgs couplings, needed for the present study as a function of the 2HDM parameters m_{h^0} , m_{H^0} , m_{A^0} , m_{H^\pm} , $\tan \beta$, α and m_{12}^2 . These couplings follow from the scalar potential and are thus independent of the Yukawa types used; they are given by

$$\begin{aligned}
\lambda_{h^0 h^0 h^0}^{2\text{HDM}} &= \frac{-3g}{2m_W s_{2\beta}^2} \left[(2c_{\alpha+\beta} + s_{2\alpha} s_{\beta-\alpha}) s_{2\beta} m_{h^0}^2 - 4c_{\beta-\alpha}^2 c_{\beta+\alpha} m_{12}^2 \right] \\
\lambda_{H^0 h^0 h^0}^{2\text{HDM}} &= -\frac{1}{2} \frac{g c_{\beta-\alpha}}{m_W s_{2\beta}^2} \left[(2m_h^2 + m_{H^0}^2) s_{2\alpha} s_{2\beta} - 2(3s_{2\alpha} - s_{2\beta}) m_{12}^2 \right] \\
\lambda_{h^0 H^0 H^0}^{2\text{HDM}} &= \frac{1}{2} \frac{g s_{\beta-\alpha}}{m_W s_{2\beta}^2} \left[(m_{h^0}^2 + 2m_{H^0}^2) s_{2\alpha} s_{2\beta} - 2(3s_{2\alpha} + s_{2\beta}) m_{12}^2 \right] \\
\lambda_{h^0 H^\pm H^\mp}^{2\text{HDM}} &= \frac{1}{2} \frac{g}{m_W} \left[(m_{h^0}^2 - 2m_{H^\pm}^2) s_{\beta-\alpha} - \frac{2c_{\beta+\alpha}}{s_{2\beta}^2} (m_h^2 s_{2\beta} - 2m_{12}^2) \right] \\
\lambda_{h^0 A^0 A^0}^{2\text{HDM}} &= \frac{1}{2} \frac{g}{m_W} \left[(m_h^2 - 2m_{A^0}^2) s_{\beta-\alpha} - \frac{2c_{\beta+\alpha}}{s_{2\beta}^2} (m_h^2 s_{2\beta} - 2m_{12}^2) \right],
\end{aligned} \tag{7}$$

with the W boson mass m_W and the $SU(2)$ gauge coupling constant g . We have used the notation s_x and c_x as short-hand notations for $\sin(x)$ and $\cos(x)$, respectively. The mixing angle β is defined by via $\tan \beta = v_2/v_1$.

It has been shown that the 2HDM has a decoupling limit which is reached for $\cos(\beta - \alpha) = 0$ and $m_{H^0, A^0, H^\pm} \gg m_Z$ [33]. In this limit, the coupling of the CP-even h^0 to SM particles completely mimic the SM Higgs couplings including the triple coupling $h^0 h^0 h^0$. Moreover, the model possesses also an alignment limit [34], in which one of the CP-even Higgs bosons h^0 or H^0 looks like SM Higgs particle if $\sin(\beta - \alpha) \rightarrow 1$ or $\cos(\beta - \alpha) \rightarrow 1$. In the decoupling or alignment limit with $\alpha = \beta - \pi/2$, the above triple Higgs couplings reduce to the simplified form

$$\begin{aligned}
\lambda_{h^0 h^0 h^0}^{2HDM} &= \frac{-3g}{2m_W} m_{h^0}^2 = \lambda_{hhh}^{SM}, \\
\lambda_{H^0 h^0 h^0}^{2HDM} &= 0, \\
\lambda_{h^0 H^0 H^0}^{2HDM} &= \frac{g}{m_W} \left[\left(\frac{2m_{12}^2}{s_{2\beta}} - m_{H^0}^2 \right) - \frac{m_{h^0}^2}{2} \right], \\
\lambda_{h^0 H^\pm H^\mp}^{2HDM} &= \frac{g}{m_W} \left[\left(\frac{2m_{12}^2}{s_{2\beta}} - m_{H^\pm}^2 \right) - \frac{m_{h^0}^2}{2} \right], \\
\lambda_{h^0 A^0 A^0}^{2HDM} &= \frac{g}{m_W} \left[\left(\frac{2m_{12}^2}{s_{2\beta}} - m_{A^0}^2 \right) - \frac{m_{h^0}^2}{2} \right].
\end{aligned} \tag{8}$$

Furthermore, in the degenerate case with the condition $m_{H^\pm} = m_{H^0} = m_{A^0} = m_S$, all triple Higgs couplings $h^0 H^0 H^0$, $h^0 A^0 A^0$ and $h^0 H^\pm H^\mp$ have the same expression, labeled by $h^0 SS$,

$$\lambda_{h^0 SS}^{2HDM} = \frac{g}{m_W} \left[\left(\frac{2m_{12}^2}{s_{2\beta}} - m_{S^0}^2 \right) - \frac{m_{h^0}^2}{2} \right]. \tag{9}$$

2.3 Theoretical and experimental constraints

The 2HDM has several theoretical constraints which we briefly address here. In order to ensure vacuum stability of the 2HDM, the scalar potential must satisfy conditions that guarantee that its bounded from below, i.e. that the requirement $V_{2HDM} \geq 0$ is satisfied for all directions of Φ_1 and Φ_2 components. This requirement imposes the following conditions on the coefficients λ_i [35, 36]:

$$\lambda_1 > 0 \quad , \quad \lambda_2 > 0 \quad , \quad \lambda_3 + 2\sqrt{\lambda_1 \lambda_2} > 0 \quad , \quad \lambda_3 + \lambda_4 - |\lambda_5| > 2\sqrt{\lambda_1 \lambda_2}. \tag{10}$$

In addition to the constraints from positivity of the scalar potential, there is another set of constraints by requiring perturbative tree-level unitarity for scattering of Higgs bosons and longitudinally polarized gauge bosons. These constraints are taken from [37, 38]. Moreover, we also force the potential to be perturbative by imposing that all quartic coefficients of the scalar potential satisfy $|\lambda_i| \leq 8\pi$ ($i = 1, \dots, 5$).

Besides these theoretical bounds, we have indirect experimental constraints from B physics observables on 2HDM parameters such as $\tan\beta$ and the charged Higgs boson mass. It is well known that in the framework of 2HDM-II and IV, for example, the measurement of the $b \rightarrow s\gamma$ branching ratio requires the charged Higgs boson mass to be heavier than 580 GeV [39, 40] for any value of $\tan\beta \geq 1$. Such a limit is much lower for the other 2HDM types [41]. In 2HDM-I and III, as long as $\tan\beta \geq 2$, it is possible to have charged Higgs

bosons as light as 100 GeV [41, 42] while being consistent with all B physics constraints as well as with LEP and LHC limits [43–48].

We stress in passing that after the Higgs-like particle discovery, several theoretical studies have performed global-fit analysis for the 2HDM to pin down the allowed regions of parameter space both for a SM-like Higgs h^0 [49] as well as for a SM-like Higgs boson H^0 [50].

The parameter space of our benchmark scenarios in this paper is already constrained by the limits obtained from various searches for additional Higgs bosons at the LHC, and by the requirement that one of the neutral scalars should match the properties of the observed Higgs-like boson. We evaluate the former constraints with the public code `HiggsBounds` [51], and the latter with the code `HiggsSignals` [52].

Before presenting our results, we would like to mention that we have performed cross checks with the results [27] for the subclass of Yukawa corrections considered there and found perfect agreement. In order to illustrate the effect of the new physics, we have chosen four benchmark points scenarios as shown in Table 2 based on the best-fit from the latest results of Higgs data using `HiggsBounds` and `HiggsSignals` public codes.

| BP's | α | β | $m_h(\text{GeV})$ | $m_H(\text{GeV})$ | $m_A(\text{GeV})$ | $m_{H^\pm}(\text{GeV})$ |
|-------|----------|---------|-------------------|-------------------|-------------------|-------------------------|
| BP1-h | -0.30 | 1.19 | 125 | 212 | 97.7 | 178 |
| BP2-h | -0.77 | 0.79 | 125 | 694 | 512 | 592 |
| BP1-H | 1.46 | 1.35 | 95 | 125 | 170 | 135.5 |
| BP2-H | 1.24 | 1.19 | 95 | 125 | 616 | 611 |

Table 2: Selected benchmark points using Higgs data at 13 TeV with $m_h = 125$ GeV, for BP1-h and BP2-h and with $m_H = 125$ GeV, for BP1-H and BP2-H. We refer to 2HDM-type-1 and type-2 by BP1 and BP2, respectively.

It is noticed that in the scenarios of both BP1-h and BP1-H, a light charged Higgs boson less than 200 GeV can be consistent with the current LHC Higgs data.

| BP's | $\lambda_{h^0 h^0 h^0}$ | $\lambda_{H^0 h^0 h^0}$ | $\lambda_{h^0 H^0 H^0}$ | $\lambda_{h^0 H^\pm H^\mp}$ | $\lambda_{h^0 A^0 A^0}$ |
|-------|-------------------------|-------------------------|-------------------------|-----------------------------|-------------------------|
| BP1-h | 0.726 | 2.74 | -257.48 | -193.27 | 14.03 |
| BP2-h | -0.79 | -23.48 | -184.6 | -781.02 | -63.67 |
| BP1-H | -499.4 | 50.8 | 0.78 | 11.23 | 19.77 |
| BP2-H | -238.2 | -60.44 | -0.55 | 150 | 152.2 |

Table 3: Triple Higgs couplings values in GeV following benchmark points in table 2.

In Table. (3), triple Higgs couplings are tabulated. It is noticed that the triple coupling $\lambda_{h^0 H^\pm H^\mp}$ for the BP1-h and BP2-h case could be quite large. While for the case BP1-H and BP2-H, the self coupling of $\lambda_{h^0 h^0 h^0}$ could be sizable.

3 One-loop calculation and renormalization scheme

3.1 Full correction of $\phi \rightarrow b\bar{b}, \tau\tau$ with $\phi = h^0, H^0$

Calculations of higher order corrections in perturbation theory in general lead to ultra-violet (UV) divergences. The standard procedure to eliminate these UV divergences consists in renormalization of the bare Lagrangian by redefinition of couplings and fields. In the SM, the on-shell renormalization scheme is well elaborated [53–55]. For the 2HDM, several extensions of the SM renormalization scheme exist in the literature [20–22, 56]. Recently, gauge independent renormalization schemes have been proposed [57, 58], with e.g. $\overline{\text{MS}}$ renormalization for the mixing angles and the soft Z_2 breaking term in the Higgs sector [58]. In the present study, we adopt the on-shell renormalization scheme used also in [20], which is an extension of the on-shell scheme of the SM: the gauge sector is renormalized in analogy to [53, 54] concerning vector-boson masses and field renormalization; also fermion mass and field renormalization is treated in an analogous way (see also [55]).

$$e \rightarrow (1 + \delta Z_e)e \quad , \quad m_{W,Z}^2 \rightarrow m_{W,Z}^2 + \delta m_{W,Z}^2 \quad (11)$$

and for the vector-boson fields

$$Z \rightarrow Z_{ZZ}^{1/2} Z + Z_{Z\gamma}^{1/2} A \quad , \quad A \rightarrow Z_{AA}^{1/2} A + Z_{\gamma Z}^{1/2} Z \quad , \quad \text{with} \quad Z_{ij}^{1/2} = \delta_{ij} + \frac{1}{2} \delta Z_{ij} \quad (12)$$

By the on-shell definition of the electroweak mixing angle ($s_W = \sin \theta_W, c_W = \cos \theta_W$) according to $s_W^2 = 1 - m_W^2/m_Z^2$, the corresponding counterterm is determined through the W and Z mass counterterms,

$$\frac{\delta s_W^2}{s_W^2} = \frac{c_W^2}{s_W^2} \left(\frac{\delta m_Z^2}{m_Z^2} - \frac{\delta m_W^2}{m_W^2} \right) \quad , \quad \frac{\delta c_W^2}{c_W^2} = \frac{\delta m_Z^2}{m_Z^2} - \frac{\delta m_W^2}{m_W^2} \quad (13)$$

As shown in Ref. [55], the renormalization constant for charge δZ_e is obtained as

$$\delta Z_e = -\frac{1}{2} \delta Z_{AA} - \frac{s_W}{c_W} \frac{1}{2} \delta Z_{ZA} = \frac{1}{2} \Pi(0) - \frac{s_W}{c_W} \frac{\sum_T^{AZ}(0)}{m_Z^2} \quad (14)$$

with

$$\Pi(s) \equiv \frac{\sum_T^{AA}(s)}{s}. \quad (15)$$

This corresponds to the running coupling constant $\alpha(0)$ obtained at Thomson limit. As the first term in δZ_e is sensitive to the hadronic contribution, usually a non-perturbative parameter $\Delta\alpha_{\text{hadron}}^{(5)}(m_Z)$ is used to absorb the hadronic contribution, namely δZ_e is rewritten as

$$\delta Z_e(0) = \frac{1}{2} \text{Re} \Pi_{\text{hadron}}^{(5)}(m_Z^2) + \frac{1}{2} \Delta\alpha_{\text{hadron}}^{(5)}(m_Z) + \frac{1}{2} \Pi_{\text{remaining}}^{(5)}(0) - \frac{s_W}{c_W} \frac{\sum_T^{AZ}(0)}{m_Z^2} \quad (16)$$

Here we call it $\alpha(0)$. Another two schemes, $\alpha(m_z)$ and $\alpha(\sqrt{s})$, are more preferred, in which the large logarithm from leptons are also absorbed into the redefinition of running coupling constant [55, 60]. Corresponding renormalization constant is

$$\delta Z_e(\mu) = \delta Z_e(0) - \frac{1}{2}\Delta\alpha(\mu) \quad (17)$$

with

$$\Delta\alpha(\mu) = \Pi_{f \neq \text{top}}(0) - \text{Re}\Pi_{f \neq \text{top}}(\mu^2) \quad (18)$$

And the running coupling constant is replaced with

$$\alpha(\mu) = \frac{\alpha(0)}{1 - \Delta\alpha(\mu)}. \quad (19)$$

Results under these two schemes will be independent of $\log(m_e)$. In the following, we use $\alpha(m_Z)$ scheme as our default choice.

For renormalization of the Higgs sector we take over the approach used in [20], which means on-shell renormalization

- for the h^0, H^0 tadpoles, yielding zero for the renormalized tadpoles and thus $v_{1,2}$ at the minimum of the potential also at one-loop order,
- for all physical masses from the Higgs potential, defining the masses $m_{h^0}, m_{H^0}, m_{A^0}, m_{H^\pm}$ as pole masses,

whereas Higgs field renormalization is done in the $\overline{\text{MS}}$ scheme. We assign renormalization constants Z_{Φ_i} for the two Higgs doublets in (3) and counter-terms for the v_i within the doublets, according to

$$\Phi_i \rightarrow (Z_{\Phi_i})^{1/2}\Phi_i, \quad v_i \rightarrow v_i - \delta v_i, \quad (20)$$

and expand the Z factors $Z_{\Phi_i} = 1 + \delta Z_{\Phi_i}$ to one-loop order. The $\overline{\text{MS}}$ condition yields the field renormalization constants as follows for all types of models listed in Table 1:

$$\begin{aligned} \delta Z_{\Phi_1}^{\overline{\text{MS}}} &= \frac{\Delta}{32\pi^2} \left\{ \frac{-g^2}{m_W^2 t_\beta} \left(\xi_l^{A^0} \left[m_e^2 + m_\mu^2 + m_\tau^2 \right] (1 + t_\beta \xi_l^A) + N_C \xi_d^{A^0} \left[m_b^2 + m_d^2 + m_s^2 \right] (1 + t_\beta \xi_d^{A^0}) \right. \right. \\ &\quad \left. \left. - N_C \xi_u^{A^0} \left[m_c^2 + m_t^2 + m_u^2 \right] (1 - t_\beta \xi_u^{A^0}) \right) + (3g^2 + g'^2) \right\}, \\ \delta Z_{\Phi_2}^{\overline{\text{MS}}} &= \frac{\Delta}{32\pi^2} \left\{ \frac{-g^2}{m_W^2} \left(-\xi_l^{A^0} \left[m_e^2 + m_\mu^2 + m_\tau^2 \right] (t_\beta - \xi_l^{A^0}) - N_C \xi_d^{A^0} \left[m_b^2 + m_d^2 + m_s^2 \right] (t_\beta - \xi_d^{A^0}) \right. \right. \\ &\quad \left. \left. + N_C \xi_u^{A^0} \left[m_c^2 + m_t^2 + m_u^2 \right] (t_\beta + \xi_u^{A^0}) \right) + (3g^2 + g'^2) \right\}, \end{aligned} \quad (21)$$

with $\Delta = 2/(4-D) - \gamma + \log 4\pi$ from dimensional regularization, the color factor $N_C = 3$ for quarks and $N_C = 1$ for leptons, and the gauge couplings g and g' . The factors $\xi_{u,d,l}^{A^0}$ can be found in Table 1. Eq. (21) is a generalization of the work of [20] with respect to the various Yukawa structures of the 2HDM.

The renormalized self-energy of the Higgs field ϕ is the following finite combination of the unrenormalized self-energy and counter-terms,

$$\widehat{\Sigma}_\phi(k^2) = \Sigma_\phi(k^2) - \delta m_\phi^2 + (k^2 - m_\phi^2) \delta Z_\phi \quad (22)$$

with the on-shell mass counter-term δm_ϕ^2 where $\delta Z_{h^0} = s_\alpha^2 \delta Z_{\Phi_1}^{\overline{\text{MS}}} + c_\alpha^2 \delta Z_{\Phi_2}^{\overline{\text{MS}}}$ and $\delta Z_{H^0} = c_\alpha^2 \delta Z_{\Phi_1}^{\overline{\text{MS}}} + s_\alpha^2 \delta Z_{\Phi_2}^{\overline{\text{MS}}}$.

Owing to the $\overline{\text{MS}}$ field renormalization, a finite wave function renormalization has to be assigned to each external ϕ in a physical amplitude. This quantity is determined by the derivative of the renormalized self-energy $\widehat{\Sigma}'_{h^0}$ on the mass shell, given by

$$\widehat{\Sigma}'_\phi(m_\phi^2) = \Sigma'_\phi(m_\phi^2) + \delta Z_\phi. \quad (23)$$

Application to the one-loop calculation for the fermionic Higgs boson decay $\phi \rightarrow f \bar{f}$ yields the decay amplitude which can be written as follows,

$$\mathcal{M}_1 = -\frac{igm_f}{2m_W} \sqrt{\widehat{Z}_\phi} \left[\xi_f^\phi (1 + \Delta\mathcal{M}_1) + \xi_f^{\phi'} \Delta\mathcal{M}_{12} \right] \quad (24)$$

where

$$\Delta\mathcal{M}_1 = V_1^{\phi f \bar{f}} + \delta(\phi f \bar{f}), \quad (25)$$

$$\Delta\mathcal{M}_{12} = \frac{\Sigma_{\phi\phi'}(m_\phi^2)}{m_\phi^2 - m_{\phi'}^2} - \delta\alpha, \quad (26)$$

$$\widehat{Z}_\phi = \left[1 + \widehat{\Sigma}'_\phi(m_\phi^2) \right]^{-1}. \quad (27)$$

$\Delta\mathcal{M}_1$ is the sum of the one-loop vertex diagrams $V_1^{\phi f \bar{f}}$ and the vertex counter-term $\delta(\phi f \bar{f})$, $\Sigma_{\phi\phi'}$ is the ϕ - ϕ' mixing ($\phi, \phi' = (h^0, H^0)$), $\delta\alpha$ represents the counter-term for the mixing angle α , and \widehat{Z}_ϕ is the finite wave function renormalization of the external ϕ fixed by the derivative of the renormalized self-energy specified above in Eq. (23). Given the fact that the mixing angle α is an independent parameter, it can be renormalized in a way independent of all the other renormalization conditions. A simple renormalization condition for α is to require that $\delta\alpha$ absorbs the transition ϕ - ϕ' in the non-diagonal part $\Delta\mathcal{M}_{12}$ of the fermionic Higgs decay amplitude. Therefore, the angle α is hence the CP-even Higgs-boson mixing angle also at the one-loop level, and the decay amplitude \mathcal{M}_1 simplifies to the $\Delta\mathcal{M}_1$ term only.

The amplitude given in Eq. (24) together with its ingredients is a generalization of the work in [20], extended to all charged fermions and for the various 2HDM types. $\Delta\mathcal{M}_1$ contains besides the genuine vertex corrections the counter-term $\delta(\phi f \bar{f})$ for Higgs-fermion-fermion vertex, which reads as follows,

$$\delta(\phi f \bar{f}) = \frac{\delta m_f}{m_f} + \delta Z_V^f + \frac{\delta v}{v}, \quad (28)$$

where

$$\frac{\delta m_f}{m_f} + \delta Z_V^f = \Sigma_S^f(m_f^2) - 2m_f^2 \left[\Sigma_S^b(m_f^2) + \Sigma_V^f(m_f^2) \right] \quad (29)$$

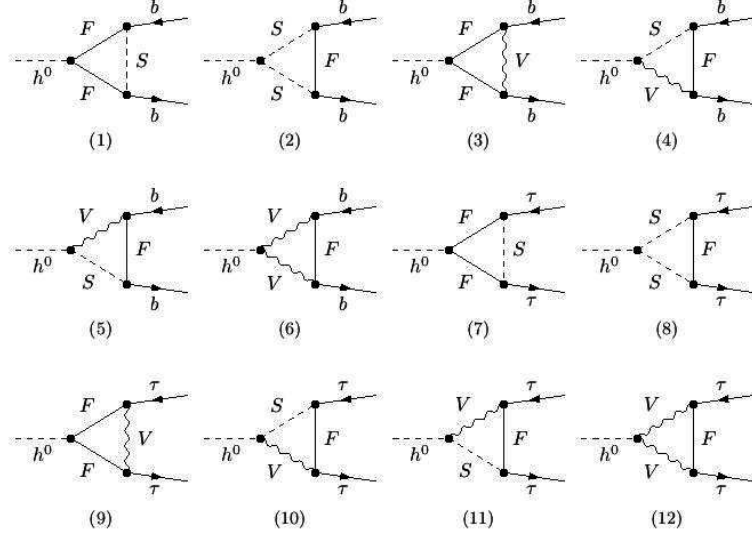


Figure 1: Generic one-loop 2HDM Feynman diagrams contributing to $\Gamma_1(h^0 \rightarrow b\bar{b})$ and $\Gamma_1(h^0 \rightarrow \tau^+\tau^-)$.

can be expressed in terms of the scalar functions of the fermion self-energy,

$$\Sigma^f(p) = \not{p} \Sigma_V^f(p^2) + \not{p} \gamma_5 \Sigma_A^f(p^2) + m_f \Sigma_S^f(p^2), \quad (30)$$

and the universal part

$$\begin{aligned} 2 \frac{\delta v}{v} = 2 \frac{\delta v_{1,2}}{v_{1,2}} &= c_\beta^2 \delta Z_{\Phi_1}^{\overline{\text{MS}}} + s_\beta^2 \delta Z_{\Phi_2}^{\overline{\text{MS}}} \\ &+ \Sigma'_{\gamma\gamma}(0) + 2 \frac{s_W}{c_W} \frac{\Sigma_{\gamma Z}(0)}{m_Z^2} - \frac{c_W^2}{s_W^2} \frac{\Re \Sigma_{ZZ}(m_Z^2)}{m_Z^2} + \frac{c_W^2 - s_W^2}{s_W^2} \frac{\Re \Sigma_{WW}(m_W^2)}{m_W^2}. \end{aligned} \quad (31)$$

This universality is a consequence of the renormalization condition

$$\frac{\delta v_1}{v_1} - \frac{\delta v_2}{v_2} = 0 \quad (32)$$

(see the discussion in [20]), which is also used in the Minimal Supersymmetric SM (MSSM), see e.g. [62–64]. It is important that the singular part of the difference in the lhs. of (32) vanishes. The singular part of δv is $(\delta v/v)_{\overline{\text{MS}}} = -\frac{1}{64\pi^2}(3g^2 + g'^2)\Delta$, which is equal to the expression found in the MSSM and constitutes a check of our calculation. We end this section by showing in Fig. (1) the one-loop Feynman diagrams in 2HDM for simplicity we draw $h^0 \rightarrow b\bar{b}$ and $h^0 \rightarrow \tau^+\tau^-$, where S stands for (H^\pm, A^0, H^0, G^\pm) for both decays while F represents (b, t) for $h^0 \rightarrow b\bar{b}$ and (τ, ν_τ) for $h^0 \rightarrow \tau^+\tau^-$. In the SM limit [33], diagrams (4, 5, 10, 11) and (2, 8) with $(S, S) = (H^\pm, G^\pm)$ vanish. Consequently, the important effects come from diagrams (1, 2) and (7, 8) respectively for $h^0 \rightarrow b\bar{b}$ and $h^0 \rightarrow \tau^+\tau^-$.

In the present work, computation of all the one-loop amplitudes and counter-terms is done with the help of FeynArts and FormCalc [65] packages. Numerical evaluations of

the scalar integrals are done with LoopTools [66]. We have also tested the cancellation of UV divergences both analytically and numerically. Before illustrating our findings, we first present the one-loop quantities that we are interested in. At one-loop order the decay width of the Higgs-boson into $b\bar{b}$ and $\tau^+\tau^-$ is given by the following expressions,

$$\Gamma_1(\phi \rightarrow f\bar{f}) = \frac{N_C \alpha m_f^2}{8s_W^2 m_W^2} \beta^3 m_\phi (\xi_f^\phi)^2 \widehat{Z}_\phi \left[1 + 2\Re(\Delta\mathcal{M}_1) \right], \quad (33)$$

where $\beta^2 = 1 - 4m_f^2/m_\phi^2$. We will parameterize the tree level width by the Fermi constant G_F , i.e. we use the relation

$$\alpha = \frac{s_W^2 m_W^2 \sqrt{2} G_F}{\pi(1 + \Delta r)} \approx \frac{s_W^2 m_W^2 \sqrt{2} G_F}{\pi} (1 - \Delta r) \quad (34)$$

where Δr incorporates higher-order corrections. According to the above relation, the one-loop decay width Eq. (33) becomes

$$\begin{aligned} \Gamma_1(\phi \rightarrow f\bar{f}) &= \frac{N_C G_F m_f^2}{4\sqrt{2}\pi} \beta^3 m_\phi (\xi_f^\phi)^2 \widehat{Z}_\phi \left[1 - \Delta r + 2\Re(\Delta\mathcal{M}_1) \right] \\ &= \Gamma_0(\phi \rightarrow f\bar{f}) \widehat{Z}_\phi \left[1 - \Delta r + 2\Re(\Delta\mathcal{M}_1) \right]. \end{aligned} \quad (35)$$

To parameterize the quantum corrections, we define the following one-loop ratios:

$$\Delta_{ff}(\phi) = \frac{\Gamma_1^{2HDM}(\phi \rightarrow f\bar{f})}{\Gamma_1^{SM}(h \rightarrow f\bar{f})} - 1, \quad (36)$$

where we also take the SM decay width $\Gamma_1^{SM}(h \rightarrow f\bar{f})$ with the one-loop electroweak corrections. The two ratios defined above will take the following form:

$$\Delta_{ff}(\phi) = \frac{\widehat{Z}_\phi (1 - \Delta r^{2HDM} + 2\Re(\Delta\mathcal{M}_1^{2HDM}))}{(1 - \Delta r^{SM} + 2\Re(\Delta\mathcal{M}_1^{SM}))} - 1, \quad f = b, \tau. \quad (37)$$

3.2 Full correction of $e^+e^- \rightarrow Zh_{SM}$ in SM

In our calculation, a small photon mass λ is introduced to regularize the soft divergence. Meanwhile, two cutoffs, ΔE and $\Delta\theta$, are introduced to deal with the IR singularities in real correction processes. Thus NLO corrections can be expressed as

$$d\sigma^{(1)} = d\sigma_V(\lambda) + d\sigma_S(\lambda, \Delta E) + d\sigma_{HC+CT}(\Delta E, \Delta\theta) + d\sigma_{H\bar{C}}(\Delta E, \Delta\theta) \quad (38)$$

where the soft part is given by

$$d\sigma_S = -\frac{\alpha}{\pi} d\sigma_0 \times \left[\log \frac{4\Delta E^2}{\lambda^2} \left(1 + \log \frac{m_e^2}{s} \right) + \frac{1}{2} \log^2 \frac{m_e^2}{s} + \log \frac{m_e^2}{s} + \frac{1}{3} \pi^2 \right], \quad (39)$$

and the $HC + CT$ part is given by

$$d\sigma_{HC+CT} \equiv d\sigma_{HC+CT}^* + d\sigma_{SC}$$

$$\begin{aligned}
d\sigma_{HC+CT}^* &= \frac{\alpha}{2\pi} \left[\frac{1+z^2}{1-z} \log \frac{\Delta\theta^2 + 4m_e^2/s}{4m_e^2/s} - \frac{2z}{1-z} \frac{\Delta\theta^2}{\Delta\theta^2 + 4m_e^2/s} \right] \\
&\quad \times \left[d\sigma_0(zk_1) + d\sigma_0(zk_2) \right] dz \\
&\xrightarrow{m_e^2 \ll \Delta\theta^2 s} \frac{\alpha}{2\pi} \left[\frac{1+z^2}{1-z} \log \Delta\theta^2 - \frac{2z}{1-z} \right] \times \left[d\sigma_0(zk_1) + d\sigma_0(zk_2) \right] dz \\
d\sigma_{SC} &= -\frac{\alpha}{\pi} \log \frac{s}{4m_e^2} \left[\frac{3}{2} + 2 \log \delta_s \right] d\sigma_0
\end{aligned} \tag{40}$$

Both the soft and virtual parts are obtained with FormCalc, while the other parts are obtained with the help of FDC [67]. The λ independence have been checked when we combine the soft and virtual parts. The dependence on ΔE and $\Delta\theta$ are shown in Tables 4 and 5. In Table 4, the dependence is seen in a wide range and we choose $\delta_s = 10^{-3}$ as our default choice. In Table 5, the result becomes cut dependent when $\Delta\theta$ is smaller than 10^{-4} . It is because the approximation in Eq. (40) demands $\Delta\theta \gg m_e/\sqrt{s} \sim 2 \times 10^{-6}$. Thus we choose $\Delta\theta = 10^{-3}$ as our choice.

| $\delta_s = 2\Delta E/\sqrt{s}$ | σ_{S+V} | $\sigma_{H\bar{C}}$ | σ_{HC+CT}^* | σ_{SC} | $\sigma^{(1)}$ |
|---------------------------------|----------------|---------------------|--------------------|---------------|----------------|
| 10^{-1} | -0.7127(0) | 0.1240(0) | -0.1199(0) | 0.4794(0) | -0.2292(0) |
| 10^{-2} | -1.4347(0) | 0.5445(0) | -0.5294(1) | 1.1903(0) | -0.2293(1) |
| 10^{-3} | -2.1567(0) | 0.9788(1) | -0.9528(2) | 1.9012(0) | -0.2295(2) |
| 10^{-4} | -2.8787(0) | 1.4142(1) | -1.3772(2) | 2.6121(0) | -0.2296(2) |
| 10^{-5} | -3.6006(0) | 1.8497(2) | -1.8016(4) | 3.3230(0) | -0.2295(4) |
| 10^{-6} | -4.3227(0) | 2.2853(2) | -2.2259(5) | 4.0339(0) | -0.2293(5) |
| 10^{-7} | -5.0446(0) | 2.7208(2) | -2.6504(6) | 4.7448(0) | -0.2294(6) |
| 10^{-8} | -5.7666(0) | 3.1564(3) | -3.0746(7) | 5.4558(0) | -0.2290(8) |

Table 4: Check for ΔE independence at $\sqrt{s} = 250$ GeV (in unit of 10^{-1} pb).

One-loop radiation correction includes collinear singularities when m_e goes to zero. In our calculation electron has nonzero mass, but the singularities will not disappear. They become terms proportional to $\log(m_e)$. Some of them are cancelled when summing up virtual and real corrections, some of them are absorbed into the redefinition of running coupling constant as mentioned above, but some are remained. To deal with this, we used following fixed order electron structure function which can be derived from Eq. (11) of Ref. [68]:

$$f_{ee}(x, s) = \delta(1-x) + \frac{\alpha}{2\pi} \log \frac{s}{4m_e^2} P_{ee}^+(x, 0) \tag{41}$$

with

$$P_{ee}^+(z, 0) = \frac{1+z^2}{(1-z)_+} + \frac{3}{2} \delta(1-z), \tag{42}$$

| $\Delta\theta$ | σ_{V+S} | $\sigma_{H\bar{C}}$ | σ_{HC+CT}^* | σ_{SC} | $\sigma^{(1)}$ |
|----------------|----------------|---------------------|--------------------|---------------|----------------|
| 10^{-1} | -2.1567(0) | 0.3856(1) | -0.3604(1) | 1.9012(0) | -0.2303(1) |
| 10^{-2} | -2.1567(0) | 0.6822(1) | -0.6566(1) | 1.9012(0) | -0.2299(1) |
| 10^{-3} | -2.1567(0) | 0.9788(1) | -0.9528(2) | 1.9012(0) | -0.2295(2) |
| 10^{-4} | -2.1567(0) | 1.2751(1) | -1.2490(3) | 1.9012(0) | -0.2294(3) |
| 10^{-5} | -2.1567(0) | 1.5527(1) | -1.5452(3) | 1.9012(0) | -0.2480(3) |
| 10^{-6} | -2.1567(0) | 1.6227(2) | -1.8414(4) | 1.9012(0) | -0.4742(4) |

Table 5: Check for $\Delta\theta$ independence at $\sqrt{s} = 250$ GeV (in unit of 10^{-1} pb).

is regularized Altarelli-Parisi splitting function. One-loop structure function is used here instead of most-commonly-used resummed one to ensure the cancellation of collinear singularities. The cancellation is shown in Table 6. We vary the mass of electron with a factor of k from 2^{-4} to 2^8 and find the result unchanged. Also, we can see that singular terms only appear in σ_{V+S} and σ_{SC} parts.

3.3 Full corrections of $e^+e^- \rightarrow Z\phi$, $\phi = h^0, H^0$

In this section we calculate the one-loop radiative corrections to the Higgs-strahlung process $e^+e^- \rightarrow Z\phi$ in the SM and 2HDM. It turns out to deal with corrections of the following corrections ϕZZ which are part of the correction to double Higgs strahlung process. Those couplings are given at the tree-level by:

$$H^0 Z_\mu Z_\nu = \frac{em_W \cos(\beta - \alpha)}{s_W c_W^2} g_{\mu\nu} \quad (43)$$

$$h^0 Z_\mu Z_\nu = \frac{em_W \sin(\beta - \alpha)}{s_W c_W^2} g_{\mu\nu} \quad (44)$$

where $s_W = \sin \theta_W$ and $c_W = \cos \theta_W$ for the electroweak mixing angle θ_W . It is clear that the processes $e^+e^- \rightarrow Zh^0, ZH^0$ are complementary to the Higgs pair production ones. At the tree-level no difference in the 2HDM as compared to the MSSM. Not like in Ref [27] where they studied $e^+e^- \rightarrow Zh, ZH$ in the alignment limit with $\sin(\beta - \alpha) = 1$ and small $\tan \beta$, we instead based on the latest best-fit of α and β from LHC Higgs data. We have calculated the radiative corrections to the tree level $e^+e^- \rightarrow Zh^0, ZH^0$ processes in 2HDM in the Feynman gauge including all the particles of the model in the loops. The Feynman diagrams from 2HDM contributing to $e^+e^- \rightarrow Zh^0$ process (for simplicity we take $\phi = h^0$) are shown in Figs. 2, 3, 4 and 5 for illustrations. Since we are dealing with a processes at the one-loop level, a systematic treatment of the UV divergences have to be considered. We will use the on-shell renormalization scheme in which the input parameters coincide with the physical masses and couplings. As performed before, the counter-terms are calculated by specific renormalization conditions which allow us to cancel the UV divergences of the

| k | σ_{V+S} | $\sigma_{H\bar{C}}$ | σ_{HC+CT}^* | σ_{SC} | $\sigma^{(1)}$ |
|----------|----------------|---------------------|--------------------|---------------|----------------|
| 2^{-4} | -2.5815(0) | 0.9788(1) | -0.9528(2) | 2.3260(0) | -0.2295(2) |
| 2^{-3} | -2.4753(0) | 0.9788(1) | -0.9528(2) | 2.2198(0) | -0.2295(2) |
| 2^{-2} | -2.3691(0) | 0.9788(1) | -0.9528(2) | 2.1136(0) | -0.2295(2) |
| 2^{-1} | -2.2629(0) | 0.9788(1) | -0.9528(2) | 2.0074(0) | -0.2295(2) |
| 2^0 | -2.1567(0) | 0.9788(1) | -0.9528(2) | 1.9012(0) | -0.2295(2) |
| 2^1 | -2.0505(0) | 0.9788(1) | -0.9528(2) | 1.7950(0) | -0.2295(2) |
| 2^2 | -1.9443(0) | 0.9788(1) | -0.9528(2) | 1.6888(0) | -0.2295(2) |
| 2^3 | -1.8381(0) | 0.9788(1) | -0.9528(2) | 1.5826(0) | -0.2295(2) |
| 2^4 | -1.7318(0) | 0.9788(1) | -0.9528(2) | 1.4763(0) | -0.2295(2) |
| 2^5 | -1.6256(0) | 0.9788(1) | -0.9528(2) | 1.3701(0) | -0.2295(2) |
| 2^6 | -1.5194(0) | 0.9788(1) | -0.9528(2) | 1.2639(0) | -0.2295(2) |
| 2^7 | -1.4132(0) | 0.9788(1) | -0.9528(2) | 1.1577(0) | -0.2295(2) |
| 2^8 | -1.3070(0) | 0.9788(1) | -0.9528(2) | 1.0515(0) | -0.2295(2) |

Table 6: Check for m_e independence at $\sqrt{s} = 250$ GeV (in unit of 10^{-1} pb).

diagrams with loops. Inserting these redefinitions into the Lagrangian, we find the following counter term for $h^0 ZZ$ and $H^0 ZZ$:

$$\begin{aligned}\delta\mathcal{L}_{h^0 ZZ} &= \frac{em_W \sin(\beta - \alpha)}{s_W c_W^2} \left(\delta Z_e + \frac{s_W^2 - c_W^2}{c_W^2 s_W} \delta s_W + \frac{\delta m_W^2}{2m_W^2} + \frac{1}{2} \delta Z_{h^0} + \frac{1}{2} \delta Z_Z \right. \\ &\quad \left. + \frac{1}{2} \cot(\beta - \alpha) \delta Z_{H^0 h^0} + \sin \beta \cos \beta \cot(\beta - \alpha) \frac{\delta \tan \beta}{\tan \beta} \right) h^0 Z^\mu Z^\nu g_{\mu\nu} \quad (45)\end{aligned}$$

$$\begin{aligned}\delta\mathcal{L}_{H^0 ZZ} &= \frac{em_W \cos(\beta - \alpha)}{s_W c_W^2} \left(\delta Z_e + \frac{s_W^2 - c_W^2}{c_W^2 s_W} \delta s_W + \frac{\delta m_W^2}{2m_W^2} + \frac{1}{2} \delta Z_{H^0} + \frac{1}{2} \delta Z_Z \right. \\ &\quad \left. + \frac{1}{2} \tan(\beta - \alpha) \delta Z_{H^0 h^0} - \sin \beta \cos \beta \tan(\beta - \alpha) \frac{\delta \tan \beta}{\tan \beta} \right) H^0 Z^\mu Z^\nu g_{\mu\nu} \quad (46)\end{aligned}$$

The Feynman diagrams for the one-loop virtual contributions are displayed in Figures. 2, 3, 4 and 5. These comprise the corrections to the initial-state vertices $(\gamma, Z)e^+e^-$ Fig (2) and the box contributions Fig (3) and corrections to photon and Z propagators and their mixing Fig (4). In the generic notation, V, S, F denote all insertions of vector, scalar and fermionic states. Note that contributions coming from initial state $e^+e^-\phi$ vertices vanish for $m_e \rightarrow 0$ since e^+ and e^- are both one-shell. A similar argument hold for the A^0 and neutral Goldstone-boson exchange diagrams. Diagrams like v_{23} and v_{28} in Fig (2) and b_{15} of Fig (3) are IR divergent when the exchanged gauge boson is a photon. For an IR-finite cross section we deal it the same as in SM.

In the limit of vanishing electron mass, The differential LO cross section for unpolarized particles is given by

$$\frac{d\sigma_0}{d\Omega} = \frac{1}{4} \frac{\sqrt{\lambda}}{64\pi^2(s - m_Z^2)^2} \sum_{spin} |\bar{v} A^\mu \varepsilon_\mu u|^2 \quad (47)$$

where $\sqrt{\lambda} = s \sqrt{(1 - \frac{(m_Z + m_\phi)^2}{s})(1 - \frac{(m_Z - m_\phi)^2}{s})}$ and the amplitudes A^μ are given in [59]. The part of the amplitude following from the one-loop diagrams, \mathcal{M}^1 , can be projected on the two invariants $P_{L,R}$ as

$$\mathcal{M}^1 = \mathcal{M}_L^1 P_L + \mathcal{M}_R^1 P_R + \dots \quad (48)$$

The omitted terms are of the type $\bar{v}(1 \pm \gamma_5)u$; they vanish in the interference with \mathcal{M}_0 and are hence not required at one-loop order. For the counterterm part of the amplitude, $\delta\mathcal{M}^1$, the projection on these two invariants is exact,

$$\delta\mathcal{M}^1 = \delta\mathcal{M}_L^1 P_L + \delta\mathcal{M}_R^1 P_R. \quad (49)$$

The NLO differential cross section can be written as follows,

$$\frac{d\sigma_1}{d\Omega} = \frac{d\sigma_0}{d\Omega} + \{ 2 \Re[\mathcal{M}_0^*(\mathcal{M}^1 + \delta\mathcal{M}^1)] + |\mathcal{M}^1 + \delta\mathcal{M}^1|^2 \} \cdot \frac{1}{4} \frac{\sqrt{\lambda}}{64\pi^2(s - m_Z^2)^2} \quad (50)$$

(spin summation to be understood) with the Born cross section from Eq. (47). At one-loop order, only the interference term contributes,

$$\Re[\mathcal{M}_0^*(\mathcal{M}^1 + \delta\mathcal{M}^1)] = [\mathcal{M}_L^0(\mathcal{M}_L^1 + \delta\mathcal{M}_L^1) + \mathcal{M}_R^0(\mathcal{M}_R^1 + \delta\mathcal{M}_R^1)] \frac{s^2}{4} \lambda \sin^2 \theta, \quad (51)$$

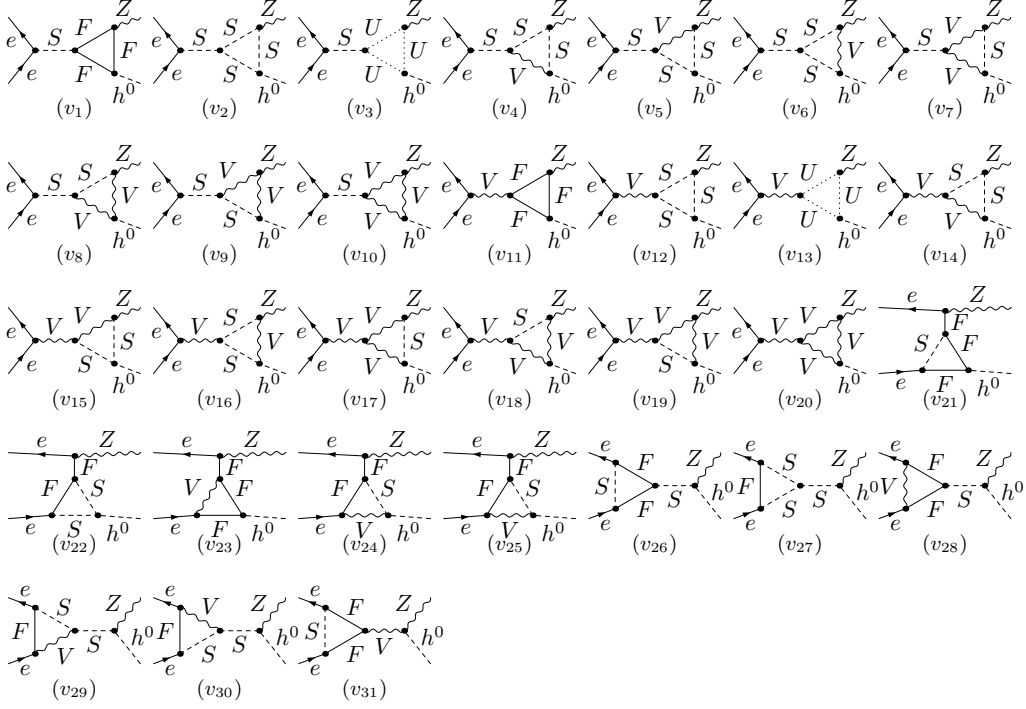


Figure 2: Generic vertices one-loop 2HDM Feynman diagrams contributing to $e^+e^- \rightarrow Zh^0$ (we take $\phi = h^0$).

on which our numerical analysis is based. Nevertheless, we will comment also on the purely-quadratic term,

$$|\mathcal{M}^1 + \delta\mathcal{M}^1|^2 = (|\mathcal{M}_L^1 + \delta\mathcal{M}_L^1|^2 + |\mathcal{M}_R^1 + \delta\mathcal{M}_R^1|^2) \frac{s^2}{4} \lambda \sin^2 \theta, \quad (52)$$

which may be useful to give some partial information on the size of higher-order corrections of $\mathcal{O}(\alpha^2)$.

The integrated cross section at the one-loop level, σ_1 , derived from Eq. (50) with the interference term only, can be written in the following way,

$$\sigma_1 = \sigma_0 + \sigma_0 \delta, \quad (53)$$

The relative correction δ in Eq.(53) can be decomposed into the following parts, indicating their origin,

$$\delta = \delta_{\text{self}} + \delta_{\text{vertex}} + \delta_{\text{boxes}} + \delta_{\text{QED}} \quad (54)$$

The electroweak terms δ_{vertex} and δ_{boxes} do not contain any virtual-photon diagram. According to the discussion at the end of section.3.2, all virtual-photon diagrams for vertex, box, and external wave-function contributions have been properly separated and combined with real bremsstrahlung to form the subclass of QED corrections, described by δ_{QED} . The analytical expression for the soft photon Bremsstrahlung can be found in [55]

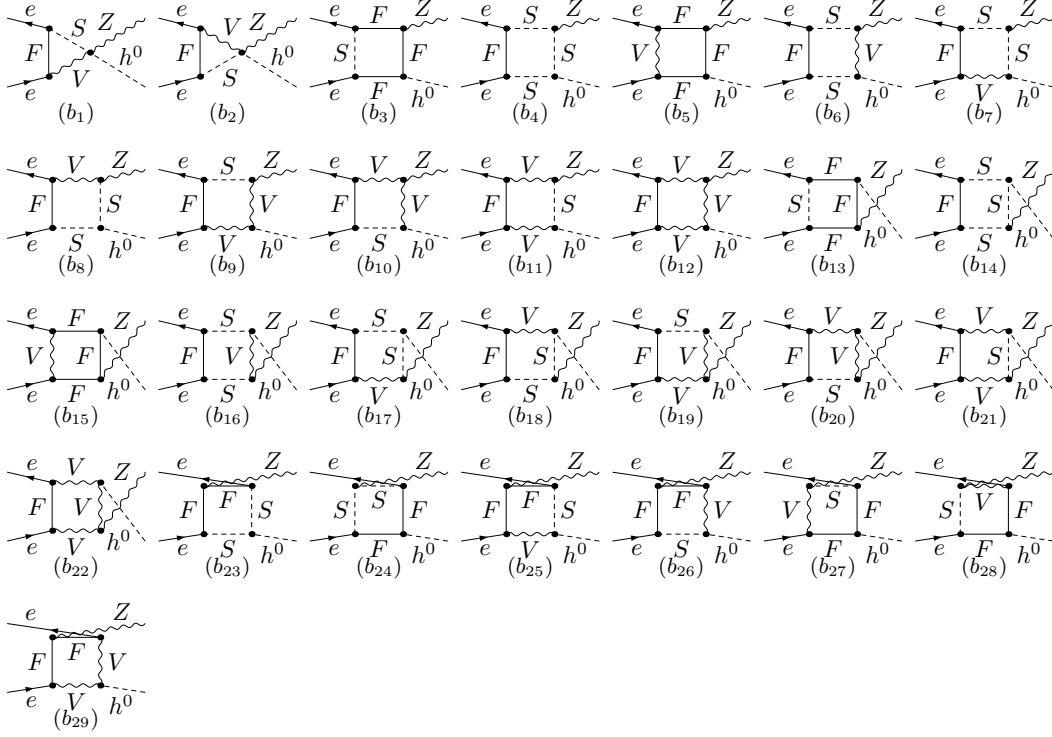


Figure 3: Generic boxes one-loop 2HDM Feynman diagrams contributing to $e^+e^- \rightarrow Zh^0$ (we take $\phi = h^0$).

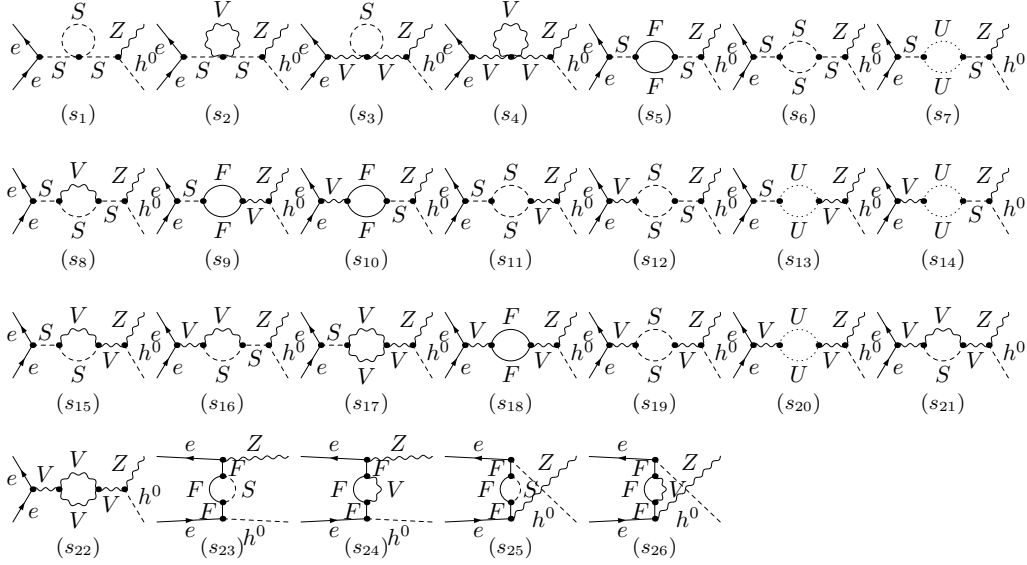


Figure 4: Generic self-energies one-loop 2HDM Feynman diagrams contributing to $e^+e^- \rightarrow Zh^0$ (we take $\phi = h^0$).

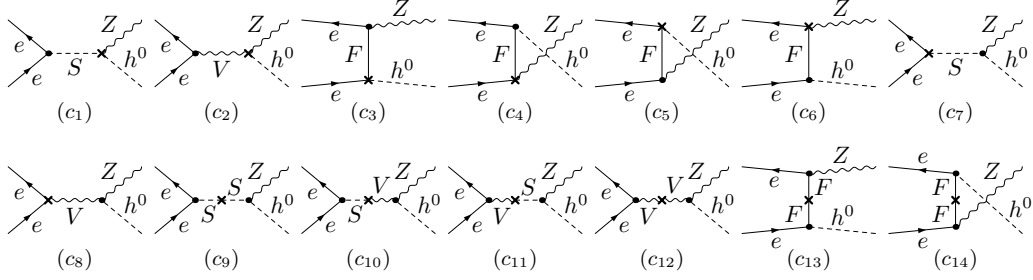


Figure 5: Generic counter-terms one-loop 2HDM Feynman diagrams contributing to $e^+e^- \rightarrow Zh^0$ (we take $\phi = h^0$).

4 Numerical results and discussions

In this section, we describe in detail the numerical results that are obtained from the analysis of the processes $e^+e^- \rightarrow Z + h/H$ at one loop level in the SM and 2HDM. Basically, we concern with the following two quantities: the ratio of the weak corrections and the ratio of the full one loop corrections (including real emissions) to the leading order results are shown. The ratio of the weak corrections is defined as:

$$\delta\sigma^{(weak)} = \frac{\sigma^{weak}}{\sigma^{(0)}}, \quad (55)$$

where σ^{weak} denotes the 1-loop weak corrections and $\sigma^{(0)}$ is the tree-level contribution of the SM and the 2HDM, respectively. The ratio of the full next-to-leading order results is defined as:

$$\delta\sigma^{(NLO)} = \frac{\sigma^{(1)}}{\sigma^{(0)}}, \quad (56)$$

where $\sigma^{(1)}$ denotes the full 1-loop corrections including real emissions

The total cross section for $e^+e^- \rightarrow Zh_{SM}$ at NLO including the real emissions can be found in Table 7. The result under $\alpha(0)$ scheme still depends on $\log(m_e)$ while the other two are independent. We can see that scale dependence has been greatly improved at NLO. And our results for weak part are consistent with those in Ref. [60].

In Fig. (6), the dependence on the renormalization scale μ and the collision energy of the cross section are shown. In Fig. (6(a)), it is noticed that the leading order results can change drastically when the unphysical renormalization scale μ varies from 0 to \sqrt{s} , i.e. the difference between the results of $\alpha(0)$ and $\alpha(\sqrt{s})$ can reach up to 15% as given in Table (7). In contrast, the next-leading order results are improved a lot. For example, the difference between the results of $\alpha(0)$ and $\alpha(\sqrt{s})$ can only reach 1% or so. In Fig. (6(b)), the lineshapes of the cross section at the leading order varying with the collision energy \sqrt{s} are shown. The largest difference between different renormalization scales occur near the threshold. The larger the collision energy \sqrt{s} goes, the less the difference between the results of different renormalization scales.

In Fig. (7), we compare the results of leading order and the full next leading order. In Fig. (7(a)), the distribution of the transverse momentum of Higgs boson in the process $e^+e^- \rightarrow Zh$ is shown. It is noticed that the lineshapes of the leading and full next leading order results are similar except a global scaling factor. In Fig. (7(b)), the cross section with

the vary of collision energy is shown. It is noticed that when $\sqrt{s} < 700$ GeV, the cross section of the full next leading order is typically smaller than the one of the leading order, but when $\sqrt{s} > 700$ GeV, the cross section of the full next leading order becomes larger, though the difference is not dramatic.

| scheme | $1/\alpha(\mu)$ | $\sigma^{(0)}$ | σ^{weak} | $\sigma^{(1)}$ | $\sigma^{(0)} + \sigma^{(1)}$ |
|--------------------|-----------------|----------------|-----------------|----------------|-------------------------------|
| $\alpha(0)$ | 137.036 | 223.12(0) | 6.09(0) | 7.22(2) | 230.34(2) |
| $\alpha(M_Z)$ | 128.943 | 252.00(0) | -24.33(0) | -22.95(2) | 229.05(2) |
| $\alpha(\sqrt{s})$ | 127.515 | 257.68(0) | -30.92(0) | -29.51(2) | 228.17(2) |

Table 7: NLO SM results under different schemes at $\sqrt{s} = 250$ GeV (in unit of fb)

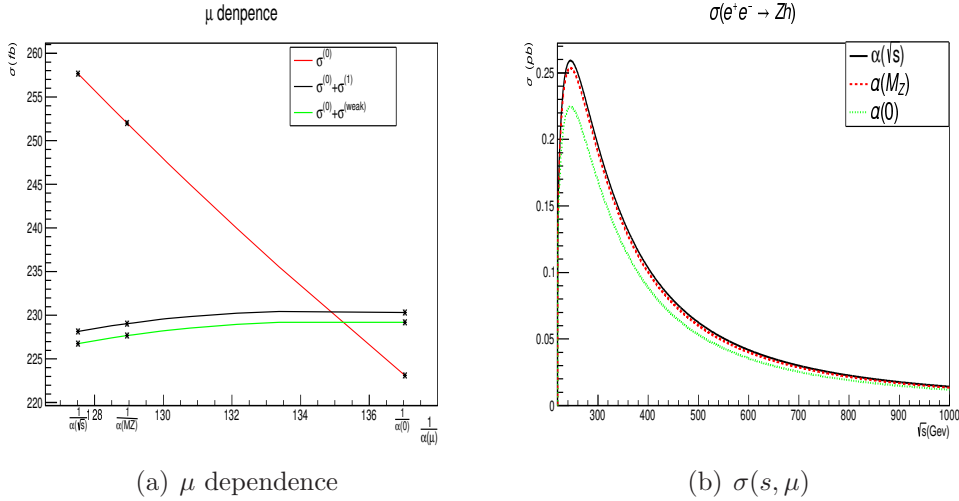


Figure 6: The dependence on the renormalization scale μ of the cross section at the leading order and NLO is examined and the dependence on the collision energy of the cross sections is shown.

Due to the constraints from the conditions of vacuum stability and the unitarity conditions of perturbation to the theoretical parameters, it is noticed that the parameter λ_5 is allowed to vary in the range from -1 to 1 or so in type-I, and from 1 to 9 or so in type-II at the process $e^+e^- \rightarrow Zh$, respectively. For the same reasons, the parameter λ_5 is allowed to vary in the range from -0.5 to 0.3 or so in type-I and from -0.6 to 0.3 or so in type-II at the process $e^+e^- \rightarrow ZH$. The parameter of λ_5 is related to the triple Higgs boson couplings, which is given as [33]

$$\lambda_5 = \frac{m_{12}^2 - m_A^2 s_\beta c_\beta}{v^2 s_\beta c_\beta} \quad (57)$$

Once λ_5 is fixed, then triple Higgs boson couplings are fixed, as shown in Eq. (7). To demonstrate the effects of triple Higgs boson self-couplings, we take a few typical values of

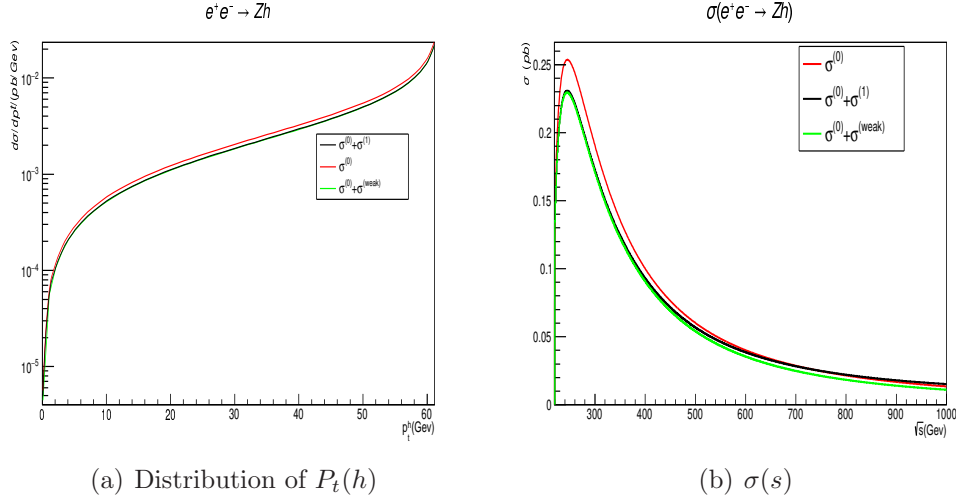


Figure 7: The distribution of the transverse momentum of Higgs boson, $P_t(h)$, and the lineshapes of cross sections at leading order and next leading order are shown. For the purpose of comparison, we choose the $\alpha(M_z)$ scheme for the leading order results.

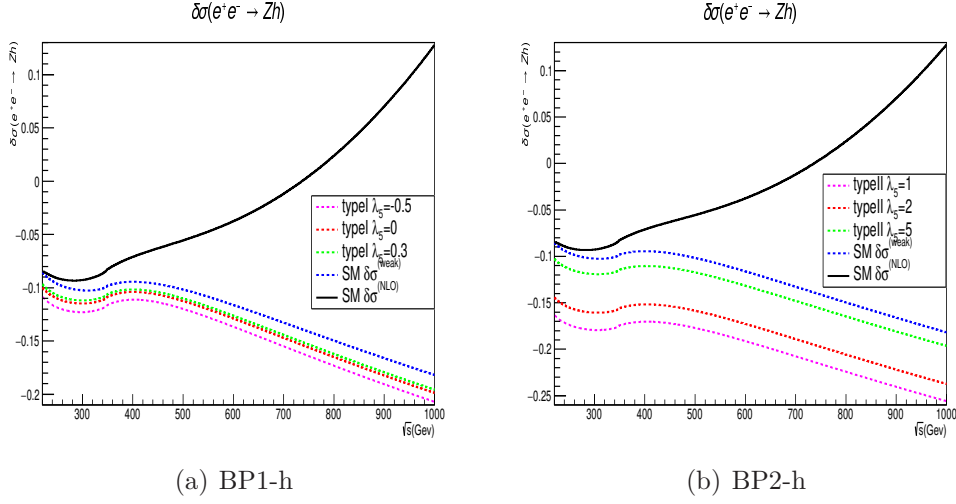


Figure 8: Process $e^+e^- \rightarrow Zh$ for bench mark points BP1-h and BP2-h. The ratios of weak corrections to the leading order results varying with the collision energy are shown. A few values of λ_5 are taken to show the effects of new physics.

$\lambda_5 = -0.5$, $\lambda_5 = 0$ and $\lambda_5 = 0.3$ in Fig. (8(a)) and $\lambda_5 = 1$, $\lambda_5 = 2$ and $\lambda_5 = 5$ Fig. (8(b)), respectively.

In Fig.(8), results of the ratios in Eq.(55) and Eq. (56) are shown, where the result of the SM at the leading order is computed with the renormalization scheme $\alpha(M_z)$ and the $h = h_{SM}$. The NLO results of SM include both the weak correction and the real emission. It is noticed that signs of the real emission and the weak interaction are different in the SM. More remarkable, the real emission becomes more and more important when the collision energy increases, as clearly shown in Fig. (8(a)). For example, when $\sqrt{s} = 250$ GeV, the contribution of real emission is small. While when $\sqrt{s} = 1$ TeV, the weak correction is around -20% , but the real emission becomes much more important and can reach $+30\%$. From the Fig. (8(b)), it is noticed that all the lines have a bump near the collision energy 350-400 GeV, which can be attributed to the contribution of top quark pair in the loop functions.

The contribution of new physics tends to further decrease the contribution of weak correction of the SM, as shown in Fig. (8) with three typical values of the parameter λ_5 . It is noticed from Fig. (8) that the larger the value of λ_5 , the smaller is the correction, which is due to the cancellation in the triple Higgs couplings, i.e. a larger the value of λ_5 corresponds a smaller triple Higgs boson couplings given in Eq. (7), as demonstrated in table (3).

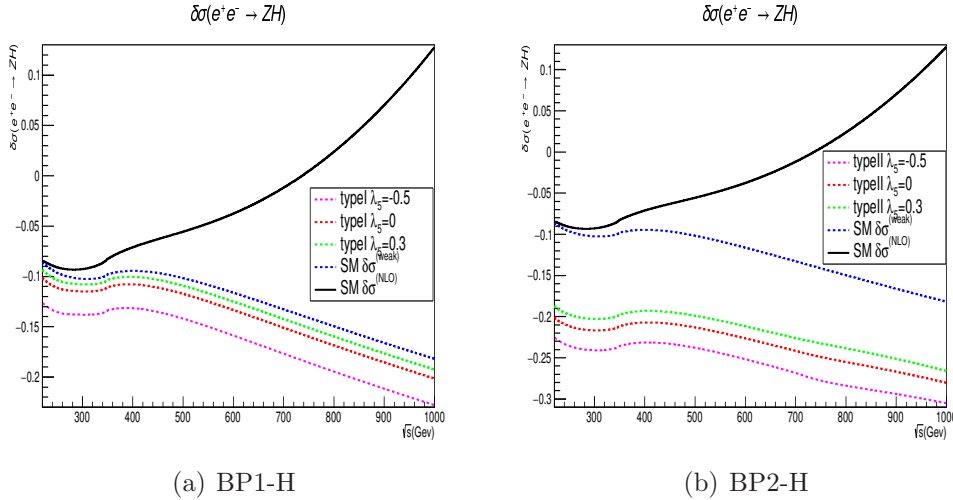


Figure 9: Process $e^+e^- \rightarrow ZH$ for bench mark points BP1-H and BP2-H. The ratios of weak corrections to the leading order results varying with the collision energy are shown. A few typical values of λ_5 are taken to show the effects of new physics.

In Fig. (9), two benchmark points for an alternative interpretation of the SM-like Higgs boson are considered, in this scenario the heavy CP even Higgs boson has a mass near 125 GeV. The detailed information on the mass spectra and parameters of these two bench mark points are presented in Table (2) and labelled as BP1-H and BP2-H. We take three typical values of $\lambda_5 = -0.5$, $\lambda_5 = 0$, and $\lambda_5 = 0.3$, respectively. It is noticed that the contributions of the first benchmark for different typical values of λ_5 increase from -10% to -20% , while those of the second benchmark changed from -20% to -30% or so due to the large contribution of Higgs boson's loop.

Furthermore, it is noticed that the weak corrections of 2HDM for these two benchmark points and the typical values of λ_5 have the same sign to those of SM, which is hold for both the type-I and type-II as well as for the process $e^+e^- \rightarrow Zh$ and $e^+e^- \rightarrow ZH$.

The last but not the least, it is noticed that all the lines have a bump near the collision energy 350-400 GeV, which can be attributed to the contribution of top quark pair in the loop functions.

In Fig. (10) and (11) we present the contribution of new physics Δ_{Zh}^{EW} and Δ_{ZH}^{EW} , respectively for different values λ_5 . The quantity Δ^{EW} is defined as given below

$$\Delta^{EW} = \frac{\sigma_{2HDM}^0 + \sigma_{2HDM}^{1,EW}}{\sigma_{SM}^0 + \sigma_{SM}^{1,EW}} - 1, \quad (58)$$

which is to describe the contribution of new physics compared with the results of the SM but the real emission is not taken into account. Obviously, the pure contribution of the SM is subtracted in this quantity, but the interferences between the new physics and the SM are counted.

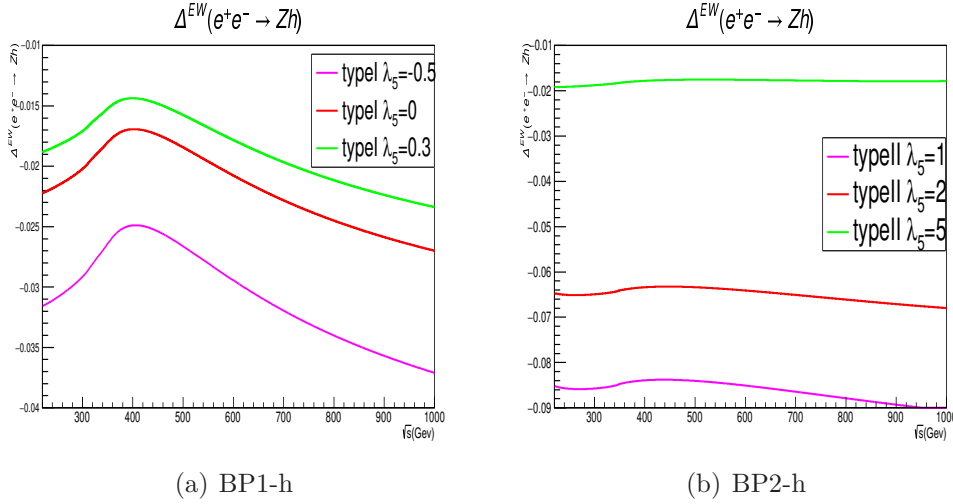


Figure 10: Process $e^+e^- \rightarrow Zh$. The 2HDM weak corrections varying with the collision energy are shown. A few values of λ_5 are taken to show the effects of new physics.

In Fig. (10), the benchmark points BP1-h and BP2-h are considered. In Fig. (10(a)), there is a bump near the 380 GeV or so, which is due to the contribution of charged Higgs bosons. In Fig. (10(b)), there is a little bump near the 350 GeV, which is due to the contribution of interference of the SM and the new physics. For BP2-h, the contribution of Higgs sector is almost constant and does not change with collision energy.

In Fig. (11), the bench mark points BP1-H and BP2-H are considered. In Fig. (11(a)), there is a bump near the 270 GeV or so, which is due to the contribution of charged Higgs bosons. In Fig. (11(b)), there are a little bump near the 350 GeV, which is due to the contribution of interference of the SM and the new physics. The change of λ_5 can change Δ^{EW} a few percent. Furthermore, there is a little dip near 730 GeV or so, which is due to the contribution of $H - A$ via the diagram s_{12} and s_{19} in Fig. (4). For BP2-H, the contribution of Higgs sector is almost constant and does not change with collision energy.

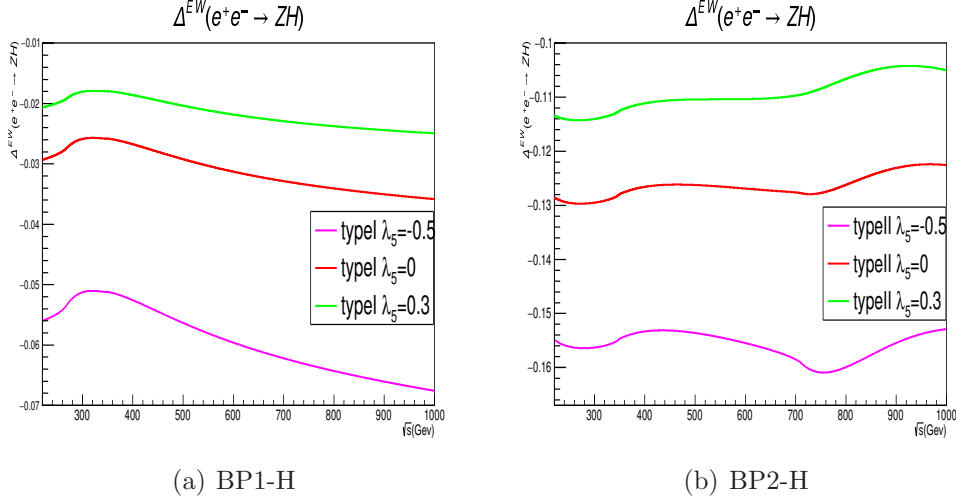


Figure 11: Process $e^+e^- \rightarrow ZH$. The 2HDM weak corrections varying with the collision energy are shown. A few typical values of λ_5 are taken to show the effects of new physics.

In Figure.(12), we discuss numerically the correlations of $\Delta_{bb}(h^0)$ and $\Delta_{\tau\tau}(h^0)$ in four types of 2HDMs for λ_5 and $\tan\beta$ in the ranges $[-2, 2]$, $[1, 5]$ respectively, the results are given for $\cos(\beta - \alpha) \leq 0$ (blue point) and ≥ 0 (black points) are shown. Our results are in good agreements with [10, 11]. Red and yellow ellipse indicate the expected prediction at $\pm 1\sigma$ at HL-LHC and CEPC, respectively. In each plot, the point (0,0) corresponds to the SM. Predictions of all the types get close to the expected precision except for 2HDM-type-II. It turns out that if $\cos(\beta - \alpha)$ change the sign, $\Delta_{bb}(h^0)$ and $\Delta_{\tau\tau}(h^0)$ for each type lead to deviate in different directions. Therefore we can determine the sign of $\cos(\beta - \alpha)$ by using a precise measurements of $b\bar{b}$ and $\tau\tau$. However it difficult to discriminate the types of 2HDMs by evaluating on $h^0 \rightarrow b\bar{b}$ and $h^0 \rightarrow \tau\bar{\tau}$ because behaviors of $\Delta_{bb}(h^0)$ and $\Delta_{\tau\tau}(h^0)$ depend on the sign of $\cos(\beta - \alpha)$. At HL-LHC, $h^0\tau\tau$ and h^0bb couplings are expected to be measured with about 8% and 11%, respectively depending on $\tan\beta$. In that case, we can discriminate the types of Yukawa interactions by using HL-LHC. At the CEPC, however, the Higgs couplings measurements have typically $\mathcal{O}(1)\%$ level resolution: *e.g* h^0 couplings to b and τ can determine in type-III and IV, respectively.

In Figure.(13), we focus on the heavy Higgs H is SM-like and whether we can distinguish it from h^0 SM-like case using the Higgs couplings measurements. Areas of the 1σ accuracy from the fiducial points are shown. In this Figure, it is clear that by using precision measurements of the Higgs boson couplings, we can distinguish H -SM-like from h -SM-like in all types of 2HDM. We note that the fiducial points in all types have a large radiative corrections which may be excluded by the sensitivity for $Hb\bar{b}$ and $H\tau\tau$ because the ratios of decay rate for the fermion are different, therefore we may be able to distinguish the H -SM-like case by the very precise measurement of the Higgs boson couplings if the integrated luminosity is large enough.

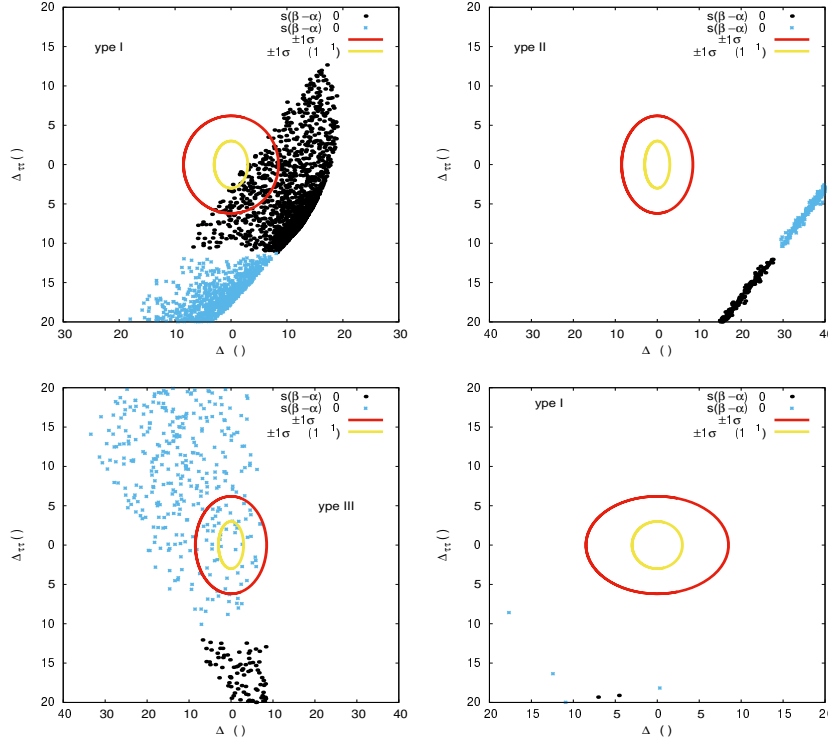


Figure 12: Correlation between relative precisions $\Delta_{\tau\tau}(h^0)$ and $\Delta_{bb}(h^0)$ in 2HDM. The ellipse show the 68% confidence regions for these couplings expected from the HL-LHC and CEPC [12].

5 Conclusion

We proposed 4 benchmark scenarios of the 2HDM after taking into account the current Higgs data from the LHC. And we have evaluated the radiative corrections to the process $e^+e^- \rightarrow Z\phi$ in the SM and in these 4 benchmark scenarios up to one-loop level.

We have used an on-shell renormalization scheme for all parameters except for wave function renormalization of the Higgs doublet which has been done in the $\overline{\text{MS}}$ scheme. Using it, we also compute the decays $\phi \rightarrow b\bar{b}$ and $\phi \rightarrow \tau^+\tau^-$ with $\phi = h^0$ and H^0 in the four types of 2HDM given in Table (1) by including the EW corrections. We have shown that in type II and IV the electroweak radiative corrections in these two decay processes are rather small due to the heavy states A^0 , H^0 and H^\pm have a mass of order of 600 GeV while they could be sizable for 2HDM type I and III, as shown in Fig. (12) and Fig. (13).

Our results demonstrate that e^+e^- colliders (especially the Higgs factories with $\sqrt{s} = 250$ GeV) can offer us the potential capability to distinguish between various 2HDM models by looking at these quantum effects in Higgs observables. As demonstrated in the Table (2), except performing precision measurements, linear colliders also have the potential to discover new physics. For example, it is possible to discover the light charged Higgs boson in BP1-h and BP1-H via $e^+e^- \rightarrow H^+H^-$ processes.

Obviously, the energy scan of e^+e^- colliders can also help to detect the mass spectra of

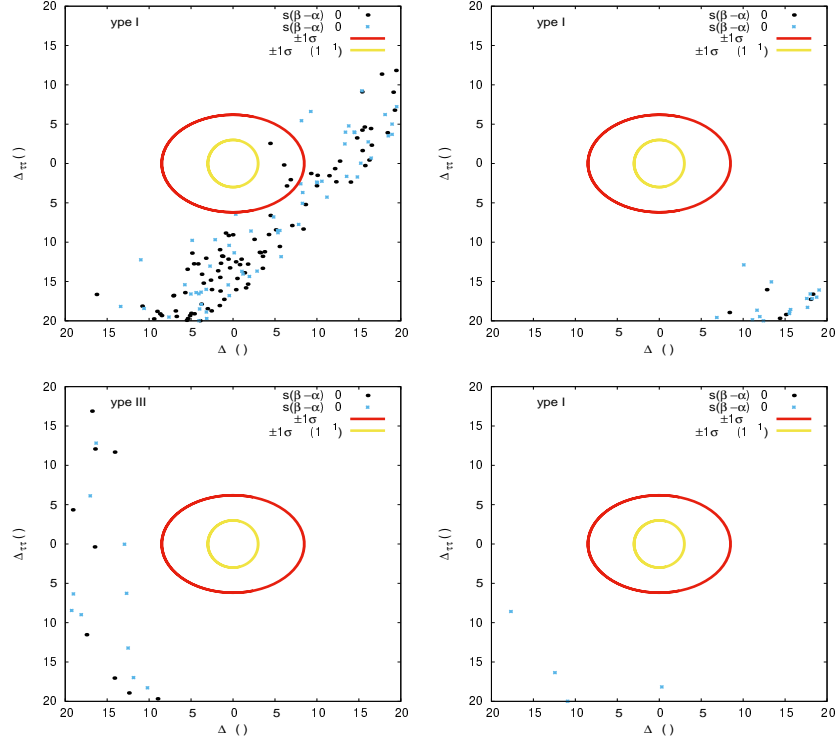


Figure 13: Correlation between relative precisions $\Delta_{\tau\tau}(H^0)$ and $\Delta_{bb}(H^0)$ in 2HDM. The coding color is the same as in Fig.12.

Higgs bosons and even triple couplings of Higgs bosons, as shown in Fig. (10) and Fig. (11). It is hopeful to reconstruct the sector of Higgs potential after combining all the future data of production and decay. Our benchmark points show that it is also possible to explore new physics beyond the SM, even if some new particles could not be directly produced in the future experiments.

Acknowledgments

We thank Abdesslam Arhrib and David Lopez-Val for helpful discussion at the early stage of this work. This work is supported by the Moroccan Ministry of Higher Education and Scientific Research MESRSFC and CNRST: Projet PPR/2015/6. RB was supported in part by the Chinese Academy of Sciences (CAS) Presidents International Fellowship Initiative (PIFI) program (Grant No. 2017VMB0021). Q.S.Yan is supported by the Natural Science Foundation of China under the grant no. 11575005. B. Gong is supported by the Natural Science Foundation of China No. 11475183.

References

- [1] G. Aad *et al.* [ATLAS Collaboration], Phys. Lett. B **716** (2012) 1 doi:10.1016/j.physletb.2012.08.020 [arXiv:1207.7214 [hep-ex]].
- [2] S. Chatrchyan *et al.* [CMS Collaboration], Phys. Lett. B **716** (2012) 30 doi:10.1016/j.physletb.2012.08.021 [arXiv:1207.7235 [hep-ex]].
- [3] G. Aad *et al.* [ATLAS and CMS Collaborations], Phys. Rev. Lett. **114** (2015) 191803 doi:10.1103/PhysRevLett.114.191803 [arXiv:1503.07589 [hep-ex]].
- [4] M. Aaboud *et al.* [ATLAS Collaboration], Phys. Rev. D **98** (2018) no.5, 052003 doi:10.1103/PhysRevD.98.052003 [arXiv:1807.08639 [hep-ex]].
- [5] A. M. Sirunyan *et al.* [CMS Collaboration], Phys. Rev. Lett. **121** (2018) no.12, 121801 doi:10.1103/PhysRevLett.121.121801 [arXiv:1808.08242 [hep-ex]].
- [6] The ATLAS collaboration [ATLAS Collaboration], ATLAS-CONF-2018-021.
- [7] A. M. Sirunyan *et al.* [CMS Collaboration], Phys. Lett. B **779** (2018) 283 doi:10.1016/j.physletb.2018.02.004 [arXiv:1708.00373 [hep-ex]].
- [8] A. M. Sirunyan *et al.* [CMS Collaboration], Phys. Rev. Lett. **120** (2018) no.23, 231801 doi:10.1103/PhysRevLett.120.231801, 10.1130/PhysRevLett.120.231801 [arXiv:1804.02610 [hep-ex]].
- [9] M. Aaboud *et al.* [ATLAS Collaboration], Phys. Lett. B **784** (2018) 173 doi:10.1016/j.physletb.2018.07.035 [arXiv:1806.00425 [hep-ex]].
- [10] A. Arhrib, R. Benbrik, J. El Falaki and W. Hollik, Phys. Lett. B **774** (2017) 195 doi:10.1016/j.physletb.2017.09.065 [arXiv:1612.09329 [hep-ph]].
- [11] S. Kanemura, M. Kikuchi, K. Mawatari, K. Sakurai and K. Yagyu, Phys. Lett. B **783** (2018) 140 doi:10.1016/j.physletb.2018.06.035 [arXiv:1803.01456 [hep-ph]].
- [12] S. Dawson *et al.*, arXiv:1310.8361 [hep-ex]. D. Zeppenfeld, R. Kinnunen, A. Nikitenko and E. Richter-Was, Phys. Rev. D **62** (2000) 013009 doi:10.1103/PhysRevD.62.013009 [hep-ph/0002036]. F. Gianotti and M. Pepe-Altarelli, Nucl. Phys. Proc. Suppl. **89** (2000) 177 doi:10.1016/S0920-5632(00)00841-0 [hep-ex/0006016]. A. Arhrib, R. Benbrik, J. El

- Falaki and W. Hollik, Phys. Lett. B **774** (2017) 195 doi:10.1016/j.physletb.2017.09.065 [arXiv:1612.09329 [hep-ph]].
- [13] C. Englert, A. Freitas, M. M. Mhlleitner, T. Plehn, M. Rauch, M. Spira and K. Walz, J. Phys. G **41** (2014) 113001 doi:10.1088/0954-3899/41/11/113001 [arXiv:1403.7191 [hep-ph]].
 - [14] G. Moortgat-Pick *et al.*, Eur. Phys. J. C **75**, no. 8, 371 (2015) doi:10.1140/epjc/s10052-015-3511-9 [arXiv:1504.01726 [hep-ph]].
 - [15] A. Djouadi, Phys. Rept. **457** (2008) 1 doi:10.1016/j.physrep.2007.10.004 [hep-ph/0503172].
 - [16] J. F. Gunion, H. E. Haber, G. L. Kane and S. Dawson, Front. Phys. **80** (2000) 1.
 - [17] D. Y. Bardin, B. M. Vilensky and P. K. Khristova, Sov. J. Nucl. Phys. **53** (1991) 152 [Yad. Fiz. **53** (1991) 240].
 - [18] A. Dabelstein and W. Hollik, Z. Phys. C **53** (1992) 507. doi:10.1007/BF01625912
 - [19] B. A. Kniehl, Nucl. Phys. B **376** (1992) 3. doi:10.1016/0550-3213(92)90065-J
 - [20] A. Arhrib, M. Capdequi Peyranere, W. Hollik and S. Penaranda, Phys. Lett. B **579** (2004) 361 doi:10.1016/j.physletb.2003.10.006 [hep-ph/0307391].
 - [21] S. Kanemura, M. Kikuchi and K. Yagyu, Phys. Lett. B **731** (2014) 27 doi:10.1016/j.physletb.2014.02.022 [arXiv:1401.0515 [hep-ph]].
 - [22] S. Kanemura, Y. Okada, E. Senaha and C.-P. Yuan, Phys. Rev. D **70** (2004) 115002 doi:10.1103/PhysRevD.70.115002 [hep-ph/0408364].
 - [23] M. E. Peskin, arXiv:1207.2516 [hep-ph].
 - [24] A. Blondel, A. Chao, W. Chou, J. Gao, D. Schulte and K. Yokoya, arXiv:1302.3318 [physics.acc-ph].
 - [25] R. Belusevic and T. Higo, arXiv:1208.4956 [physics.acc-ph].
 - [26] H. Baer *et al.*, arXiv:1306.6352 [hep-ph].
 - [27] D. Lopez-Val, J. Sola and N. Bernal, Phys. Rev. D **81** (2010) 113005 doi:10.1103/PhysRevD.81.113005 [arXiv:1003.4312 [hep-ph]].
 - [28] G. Belanger, F. Boudjema, J. Fujimoto, T. Ishikawa, T. Kaneko, K. Kato and Y. Shimizu, Phys. Lett. B **559**, 252 (2003) doi:10.1016/S0370-2693(03)00339-3 [hep-ph/0212261].
 - [29] J. Guasch, W. Hollik and S. Penaranda, Phys. Lett. B **515**, 367 (2001) doi:10.1016/S0370-2693(01)00866-8 [hep-ph/0106027].
 - [30] E. Arganda, J. Guasch, W. Hollik and S. Penaranda, Eur. Phys. J. C **76**, no. 5, 286 (2016) doi:10.1140/epjc/s10052-016-4129-2 [arXiv:1506.08462 [hep-ph]].
 - [31] S. L. Glashow and S. Weinberg, Phys. Rev. D **15**, 1958 (1977). doi:10.1103/PhysRevD.15.1958
 - [32] G. C. Branco, P. M. Ferreira, L. Lavoura, M. N. Rebelo, M. Sher and J. P. Silva, Phys. Rept. **516**, 1 (2012) doi:10.1016/j.physrep.2012.02.002 [arXiv:1106.0034 [hep-ph]].
 - [33] J. F. Gunion and H. E. Haber, Phys. Rev. D **67**, 075019 (2003) doi:10.1103/PhysRevD.67.075019 [hep-ph/0207010].
 - [34] M. Carena, I. Low, N. R. Shah and C. E. M. Wagner, JHEP **1404**, 015 (2014) [arXiv:1310.2248 [hep-ph]].
 - [35] N. G. Deshpande and E. Ma, Phys. Rev. D **18**, 2574 (1978). doi:10.1103/PhysRevD.18.2574 M. Sher, Phys. Rept. **179**, 273 (1989). doi:10.1016/0370-1573(89)90061-6

- [36] P. M. Ferreira, R. Santos and A. Barroso, Phys. Lett. B **603**, 219 (2004) Erratum: [Phys. Lett. B **629**, 114 (2005)] doi:10.1016/j.physletb.2004.10.022, 10.1016/j.physletb.2005.09.074 [hep-ph/0406231].
- [37] S. Kanemura, T. Kubota and E. Takasugi, Phys. Lett. B **313**, 155 (1993) doi:10.1016/0370-2693(93)91205-2 [hep-ph/9303263]. S. Kanemura and K. Yagyu, Phys. Lett. B **751**, 289 (2015) doi:10.1016/j.physletb.2015.10.047 [arXiv:1509.06060 [hep-ph]].
- [38] A. G. Akeroyd, A. Arhrib and E. M. Naimi, Phys. Lett. B **490**, 119 (2000) [arXiv:hep-ph/0006035]. A. Arhrib, arXiv:hep-ph/0012353. J. Horejsi and M. Kladiva, Eur. Phys. J. C **46**, 81 (2006) [arXiv:hep-ph/0510154]. I. F. Ginzburg and I. P. Ivanov, Phys. Rev. D **72**, 115010 (2005) doi:10.1103/PhysRevD.72.115010 [hep-ph/0508020].
- [39] M. Misiak and M. Steinhauser, Eur. Phys. J. C **77**, no. 3, 201 (2017) doi:10.1140/epjc/s10052-017-4776-y [arXiv:1702.04571 [hep-ph]].
- [40] M. Misiak *et al.*, Phys. Rev. Lett. **114** (2015) no.22, 221801 doi:10.1103/PhysRevLett.114.221801 [arXiv:1503.01789 [hep-ph]].
- [41] T. Enomoto and R. Watanabe, JHEP **1605** (2016) 002 doi:10.1007/JHEP05(2016)002 [arXiv:1511.05066 [hep-ph]].
- [42] A. Arhrib, R. Benbrik and S. Moretti, Eur. Phys. J. C **77** (2017) no.9, 621 doi:10.1140/epjc/s10052-017-5197-7 [arXiv:1607.02402 [hep-ph]].
- [43] G. Aad *et al.* [ATLAS Collaboration], JHEP **1503** (2015) 088 doi:10.1007/JHEP03(2015)088 [arXiv:1412.6663 [hep-ex]].
- [44] V. Khachatryan *et al.* [CMS Collaboration], JHEP **1511**, 018 (2015) S. Chatrchyan *et al.* [CMS Collaboration], JHEP **1207**, 143 (2012) CMS Collaboration [CMS Collaboration], CMS-PAS-HIG-14-020.
- [45] V. Khachatryan *et al.* [CMS Collaboration], JHEP **1512** (2015) 178.
- [46] G. Aad *et al.* [ATLAS Collaboration], Eur. Phys. J. C **73**, no. 6, 2465 (2013).
- [47] G. Abbiendi *et al.* [ALEPH, DELPHI, L3, OPAL and LEP Collaborations], Eur. Phys. J. C **73**, 2463 (2013).
- [48] A. G. Akeroyd *et al.*, arXiv:1607.01320 [hep-ph].
- [49] P. M. Ferreira, R. Santos, M. Sher and J. P. Silva, Phys. Rev. D **85**, 077703 (2012) doi:10.1103/PhysRevD.85.077703 [arXiv:1112.3277 [hep-ph]]. J. Bernon, J. F. Gunion, H. E. Haber, Y. Jiang and S. Kraml, Phys. Rev. D **92**, no. 7, 075004 (2015) doi:10.1103/PhysRevD.92.075004 [arXiv:1507.00933 [hep-ph]]. B. Dumont, J. F. Gunion, Y. Jiang and S. Kraml, Phys. Rev. D **90**, 035021 (2014) doi:10.1103/PhysRevD.90.035021 [arXiv:1405.3584 [hep-ph]]. K. Cheung, J. S. Lee and P. Y. Tseng, JHEP **1401**, 085 (2014) doi:10.1007/JHEP01(2014)085 [arXiv:1310.3937 [hep-ph]]. O. Eberhardt, U. Nierste and M. Wiebusch, JHEP **1307**, 118 (2013) doi:10.1007/JHEP07(2013)118 [arXiv:1305.1649 [hep-ph]]. B. Coleppa, F. Kling and S. Su, JHEP **1401**, 161 (2014) doi:10.1007/JHEP01(2014)161 [arXiv:1305.0002 [hep-ph]]. A. Arhrib, R. Benbrik, C. H. Chen, M. Gomez-Bock and S. Semmlali, Eur. Phys. J. C **76**, no. 6, 328 (2016) doi:10.1140/epjc/s10052-016-4167-9 [arXiv:1508.06490 [hep-ph]]. C. W. Chiang and K. Yagyu, JHEP **1307**, 160 (2013) doi:10.1007/JHEP07(2013)160 [arXiv:1303.0168 [hep-ph]].
- [50] J. Bernon, J. F. Gunion, H. E. Haber, Y. Jiang and S. Kraml, Phys. Rev. D **93**, no. 3, 035027 (2016) doi:10.1103/PhysRevD.93.035027 [arXiv:1511.03682 [hep-ph]].

- P. M. Ferreira, R. Santos, M. Sher and J. P. Silva, Phys. Rev. D **85**, 035020 (2012) doi:10.1103/PhysRevD.85.035020 [arXiv:1201.0019 [hep-ph]].
- [51] P. Bechtle, O. Brein, S. Heinemeyer, G. Weiglein and K. E. Williams, Comput. Phys. Commun. **181** (2010) 138 doi:10.1016/j.cpc.2009.09.003 [arXiv:0811.4169 [hep-ph]].
 - [52] P. Bechtle, S. Heinemeyer, O. Stl, T. Stefaniak and G. Weiglein, Eur. Phys. J. C **74** (2014) no.2, 2711 doi:10.1140/epjc/s10052-013-2711-4 [arXiv:1305.1933 [hep-ph]].
 - [53] M. Bohm, H. Spiesberger and W. Hollik, Fortsch. Phys. **34**, 687 (1986). doi:10.1002/prop.19860341102
 - [54] W. F. L. Hollik, Fortsch. Phys. **38**, 165 (1990). doi:10.1002/prop.2190380302
 - [55] A. Denner, at LEP-200,” Fortsch. Phys. **41** (1993) 307 doi:10.1002/prop.2190410402 [arXiv:0709.1075 [hep-ph]].
 - [56] S. Hossenberger and W. Hollik, arXiv:1607.04610 [hep-ph].
 - [57] M. Krause, R. Lorenz, M. Muhlleitner, R. Santos and H. Ziesche, arXiv:1605.04853 [hep-ph].
 - [58] A. Denner, L. Jenniches, J. N. Lang and C. Sturm, arXiv:1607.07352 [hep-ph].
 - [59] J. Fleischer and F. Jegerlehner, Nucl. Phys. B **216** (1983) 469. doi:10.1016/0550-3213(83)90296-1
 - [60] Q. F. Sun, F. Feng, Y. Jia and W. L. Sang, Phys. Rev. D **96** (2017) no.5, 051301 doi:10.1103/PhysRevD.96.051301 [arXiv:1609.03995 [hep-ph]].
 - [61] A. Dabelstein, Nucl. Phys. B **456**, 25 (1995) doi:10.1016/0550-3213(95)00523-2 [hep-ph/9503443].
 - [62] A. Dabelstein, Z. Phys. C **67** (1995) 495 doi:10.1007/BF01624592 [hep-ph/9409375].
 - [63] P. H. Chankowski, S. Pokorski and J. Rosiek, Nucl. Phys. B **423** (1994) 437 doi:10.1016/0550-3213(94)90141-4 [hep-ph/9303309].
 - [64] M. Frank, T. Hahn, S. Heinemeyer, W. Hollik, H. Rzehak and G. Weiglein, JHEP **0702** (2007) 047 doi:10.1088/1126-6708/2007/02/047 [hep-ph/0611326].
 - [65] T. Hahn, Comput. Phys. Commun. **140**, 418 (2001) [hep-ph/0012260]. T. Hahn and M. Perez-Victoria, Comput. Phys. Commun. **118**, 153 (1999) [hep-ph/9807565]; T. Hahn and M. Rauch, Nucl. Phys. Proc. Suppl. **157**, 236 (2006) [hep-ph/0601248].
 - [66] G. J. van Oldenborgh, Comput. Phys. Commun. **66**, 1 (1991); T. Hahn, Acta Phys. Polon. B **30**, 3469 (1999) [hep-ph/9910227]. T. Hahn, PoS ACAT **2010**, 078 (2010) [arXiv:1006.2231 [hep-ph]].
 - [67] J. X. Wang, Nucl. Instrum. Meth. A **534** (2004) 241 doi:10.1016/j.nima.2004.07.094 [hep-ph/0407058].
 - [68] E. A. Kuraev and Victor S. Fadin, Sov. J. Nucl. Phys. **41**, 466 (1985) [Yad. Fiz. **41**, 733(1985)].